University of Alberta

Role of a Temperature-Sensitive Polymer as a Process Aid in Oil Sands Processing and Tailings Treatment

by

Hongjun Li ©

A thesis submitted to the Faculty of Graduate Studies and Research
in partial fulfillment of the requirements of the degree of Master of Science

in

Chemical Engineering

Department of Chemical and Materials Engineering

Edmonton, Alberta

Spring 2007

Library and Archives Canada

Published Heritage Branch

395 Wellington Street
Ottawa ON K1A 0N4
Canada

Bibliothèque et Archives Canada

Direction du Patrimoine de l'édition

395, rue Wellington
Ottawa ON K1A 0N4
Canada

Your file Votre référence
ISBN: 978-0-494-29985-2
Our file Notre référence
ISBN: 978-0-494-29985-2

NOTICE:
The author has granted a non-exclusive license allowing Library and Archives Canada to reproduce, publish, archive, preserve, conserve, communicate to the public by telecommunication or on the Internet, loan, distribute and sell theses worldwide, for commercial or non-commercial purposes, in microform, paper, electronic and/or any other formats.

The author retains copyright ownership and moral rights in this thesis. Neither the thesis nor substantial extracts from it may be printed or otherwise reproduced without the author's permission.

AVIS:
L'auteur a accordé une licence non exclusive permettant à la Bibliothèque et Archives Canada de reproduire, publier, archiver, sauvegarder, conserver, transmettre au public par télécommunication ou par l'Internet, prêter, distribuer et vendre des thèses partout dans le monde, à des fins commerciales ou autres, sur support microforme, papier, électronique et/ou autres formats.

L'auteur conserve la propriété du droit d'auteur et des droits moraux qui protège cette thèse. Ni la thèse ni des extraits substantiels de celle-ci ne doivent être imprimés ou autrement reproduits sans son autorisation.

In compliance with the Canadian Privacy Act some supporting forms may have been removed from this thesis.

While these forms may be included in the document page count, their removal does not represent any loss of content from the thesis.

Conformément à la loi canadienne sur la protection de la vie privée, quelques formulaires secondaires ont été enlevés de cette thèse.

Bien que ces formulaires aient inclus dans la pagination, il n'y aura aucun contenu manquant.

Canada

ABSTRACT

A temperature-sensitive polymer, Poly N-isopropylacrylamide (poly(NIPAM)), was synthesized and used as a flocculant to treat kaolinite clay suspensions and as an aid to process low-grade oil sand ores. In the settling of clay suspensions, two procedures referred to as procedures A and B, respectively, were employed. In both procedures, the polymer was first mixed with kaolinite suspensions at room temperature. In procedure A, settling tests were carried out at room temperature, i.e., without changing the mixing temperature. In procedure B, the prepared suspensions were heated to 40°C and then settling tests were carried out at this higher temperature. The results showed that procedure B resulted in significantly higher settling rates and smaller sediment volumes. While used as an aid in a low-grade oil sand ore processing, the polymer exhibited a similar behavior in the flocculation of fine particles in the ore, i.e. by adding the polymer at room temperature but operating the bitumen extraction at 40°C, significantly higher bitumen recoveries and faster tailings settling rates were achieved.

To understand the role of the polymer in the settling of clay suspensions, the long-range interaction and adhesion forces between kaolinite particles in aqueous solutions in the presence of the polymer were directly measured using an atomic force microscope (AFM). The force measurements were carried out at both room temperature and 40°C by following similar temperature-changing procedures as used in the settling tests. At 40°C, stronger adhesion and weaker long-range repulsive forces were measured. The retracting force profiles obtained at different temperatures confirmed the conformation change of the polymer with temperature.

ACKNOWLEDGEMENTS

The author wishes to express his sincerest gratitude to his supervisors: Dr. Jacob H. Masliyah and Dr. Zhenghe Xu for their excellent guidance and encouragement throughout the course of this M.Sc. Research.

Special appreciation is due to Dr. Jun Long for his valuable discussion and suggestions.

The author wishes to express his gratefulness to his wife Ms. Jia Liu for raising their child during the period of this study at the University of Alberta.

Special appreciation is extended to all members in the Oil Sands Research Group at the University of Alberta for their kind assistance during this research.

The financial support from NSERC Industrial Research Chair in Oil Sands Engineering is also gratefully appreciated.

TABLE OF CONTENTS

Chapter 1 Introduction 1

Chapter 2 Literature review 4

2.1 Current methodology of oil sands tailings management 4

2.2 Temperature-sensitive polymer flocculants 7

2.3 Oil sands processibility 10

2.3.1 Effect of oil sands ore grade 10

2.3.2 Effect of water chemistry 11

2.3.3 Effect of process aids 12

2.4 Surface force review 13

2.4.1 Electrokinetics 14

2.4.2 Long-range force 16

2.4.2.1 Electric double layer force 16

2.4.2.2 Van der Waals forces 17

2.4.2.3 Steric force 18

2.4.2.4 Hydrophobic force 19

2.4.2.5 DLVO theory 20

2.4.3 Contact adhesion force 21

2.4.3.1 Work of adhesion 21

2.4.3.2 Adhesion force between solid particles 21

2.5 Summary of literature review 23

Chapter 3 Experimental procedure 24

3.1 Polymer preparation 24

3.2 Settling tests 25

3.2.1 Clay suspension preparation 25

3.2.2 Settling Procedures 26

3.3 Oil sands extraction 27

3.3.1 Materials 27

3.3.2 Extraction procedures 28

3.4 Zeta potential measurements 29

3.5 Surface force measurement 31

3.5.1 Clay probe preparation 31

3.5.2 Substrate preparation 32

3.5.3 Surface force measurements 32

3.6 Summary 34

Chapter 4 Model system: kaolinite clays in de-ionized water 35

4.1 Molecular weight of poly(NIPAM) 35

4.2 Settling of clay suspensions prepared in de-ionized water 37

4.2.1 Settling results 37

4.2.1.1 Results from procedure A 37

4.2.1.2 Results from procedure B 39

4.2.2 AFM force measurements 42

4.2.2.1 Results obtained at room temperature 42

4.2.2.2 Results obtained at 40°C 52

4.3 Summary 63

Chapter 5 Kaolinite clays in Aurora process water 64

5.1 Settling results 64

5.1.1 Results from procedure A 64

5.1.2 Results from procedure B 67

5.2 AFM force measurement 70

5.2.1 Results obtained at room temperature 70

5.2.2 Results obtained at 40°C 74

5.2.3 Relationship of the settling results and measured adhesion forces 78

5.3 Summary 79

Chapter 6 Oil Sands System 80

6.1 Results from procedure I 80

6.2 Results from procedure II 84

6.3 Summary 89

Chapter 7 Conclusions 90

Chapter 8 Recommendations for future study 92

References 93

Appendix 102

LIST OF FIGURES

Figure 1.1 Simplified flow diagram of an oil sands extraction process. 2

Figure 2.1 Cross section of an oil sands tailings settling basis. 5

Figure 2.2 Schematic illustration of the structure change of a temperature-sensitive polymer with temperature. 8

Figure 2.3 Chemical structure of poly(NIPAM) 9

Figure 2.4 Schematic of Stern double layer model. 15

Figure 3.1 The laboratory hydrotransport extraction system (LHES). System parts: 1- Hydrotransport loop, 2-Froth collector, 3-Sample visualized tube, 4-CCD camera, 5-Air injection, 6-Circulating bath, 7-Computer, 8-Pump. 28

Figure 3.2 Schematic of zeta potential distribution measurement. 30

Figure 3.3 (a) Kaolinite clay particle probe; (b) Kaolinite clay particles glued on a flat substrate. 32

Figure 4.1 Relationship between η_{sp}/c and polymer concentration in tetrahydrofuran. 36

Figure 4.2a Settling curves of kaolinite clay suspensions at various polymer dosages at room temperature.. 38

Figure 4.2b Initial settling rate as a function of polymer dosage at room temperature..... 38

Figure 4.2c Sediment volume after 120 minutes as a function of polymer dosage at room temperature. 39

Figure 4.3a Settling curves of kaolinite suspensions at various polymer dosages at 40°C..... 40

Figure 4.3b Initial settling rate as a function of the polymer dosage at 40°C. 41

Figure 4.3c Sediment volume after a period of 120 minutes as a function of polymer dosage at 40°C..... 41

Figure 4.4 A photo showing kaolinite suspensions settling at various polymer dosages at 40°C..... 42

Figure 4.5 Long-range interaction and adhesion forces between kaolinite particles in 1mM KCl solution at pH~8.6 and room temperature. The solid curve is the DLVO force profile using ψ = -35 mV, κ^{-1} = 9.61 nm and A = 2.20×10^{-20}J. The inset shows the adhesion force distribution..... 44

Figure 4.6 Long-range interaction and adhesion forces between kaolinite particles in a 1mM KCl solution and presence of 20 ppm poly(NIPAM) at pH~8.6 and room temperature. The inset shows the adhesion force distribution. 46

Figure 4.7 (a) A typical retraction force profile obtained between kaolinite particles in a 1 mM KCl solution and presence of 20 ppm poly(NIPAM) at pH~8.6 and room temperature. (b) Distribution of the pull-off distance obtained under the same condition as (a)..... 47

Figure 4.8 Long-range interaction and adhesion forces between kaolinite particles in a 1 mM KCl solution and presence of 50 ppm poly(NIPAM) at pH~8.6 and room temperature. The inset shows the adhesion force distribution. 49

Figure 4.9 (a) Average adhesion forces as a function of polymer dosage at room temperature and pH~8.6. (b) Initial settling rate as a function of polymer dosage. 51

Figure 4.10 Long-range interaction and adhesion forces between kaolinite particles in a 1 mM KCl solution and the absence of poly(NIPAM) at pH~8.6 and 40°C. The solid curve is the DLVO force profile using κ^{-1} = 9.61 nm, A = 2.20×10^{-20} J and a fitted potential of -50 mV. The inset shows the adhesion force distribution..... 54

Figure 4.11 Long-range interaction and adhesion forces between kaolinite particles in a 1mM KCl solution at pH~8.6 and presence of 20 ppm poly(NIPAM) at 40°C. The inset shows the adhesion force distribution. 55

Figure 4.12 Long-range interaction and adhesion forces between kaolinite particles in a 1mM KCl solution at pH~8.6 and presence of 50 ppm poly(NIPAM) at 40°C. The inset shows the adhesion force distribution.....56

Figure 4.13 Typical retraction force profile obtained between kaolinite particles in a 1mM KCl solution and presence of 20 ppm poly(NIPAM) at pH~8.6 and 40°C..... 57

Figure 4.14 Role of polymer concentration in fine kaolinite flocculation (schematic). At room temperature: (a) Low polymer concentration (e.g. 20 ppm). The surface of the particles was partially covered by the adsorbed polymer molecules with a stretched structure. Bridging was formed between the two particles by the adsorbed polymers. (b) High polymer concentration

(e.g. 50 ppm). The surface of the particles was fully covered by the adsorbed polymer molecules. A steric repulsion was caused by the extruded polymer tails. At 40°C: (c) Low polymer concentration (e.g. 20 ppm). Bridging was formed between two particles by the adsorbed polymers with a coil-like structure. (d) High polymer concentration (e.g. 50 ppm). The surface coverage of the particles by the adsorbed polymers was increased. More polymer bridges were formed between the two particles by the adsorbed polymer molecules. 59

Figure 4.15 Schematic diagram of the flocculation mechanism using a temperature-sensitive polymer (poly(NIPAM) for procedure B. 60

Figure 4.16 (a) Average adhesion forces as a function of polymer dosage at 40°C. (b) Initial settling rate as a function of the polymer dosage using settling procedure B. 62

Figure 5.1a Settling curves of kaolinite clay suspensions at various polymer dosages at room temperature (procedure A). 66

Figure 5.1b Initial settling rate as a function of polymer dosage at room tempeature.. 66

Figure 5.1c Sediment volumes after a settling period of 120 minutes as a function of polymer dosages at room temperature. 67

Figure 5.2a Settling curves of kaolinite clay suspensions at various polymer dosages at 40°C (procedure B). 68

Figure 5.2b Initial settling rate as a function of polymer dosage at 40°C.. 69

Figure 5.2c Sediment volume after a settling period of 120 minutes as a function of polymer dosage at 40°C. 69

Figure 5.3 Long-range interaction and adhesion forces between kaolinite-kaolinite particles in the supernatant of the suspension in the absence of poly(NIPAM) at room temperature. The solid curve was obtained with the DLVO theory by using ψ= -27 mV, κ^{-1} = 1.52 nm and A = 2.20×10^{-20} J. The inset shows the adhesion forces distribution. 71

Figure 5.4 Long-range interaction and adhesion forces between two kaolinite particles in the supernatant of the suspension in the presence of 80 ppm polymer at room temperature. The inset shows the normalized adhesion force distribution. 72

Figure 5.5 Typical retraction force profile recorded between two kaolinite particles in the supernatant of the suspension in the presence of 80 ppm polymer at room temperature. 73

Figure 5.6 Long-range interaction and adhesion forces between two kaolinite particles in the supernatant of the suspension in the presence of 100 ppm polymer at room temperature. The inset shows the normalized adhesion force distribution. 74

Figure 5.7 Long-range interaction and adhesion forces in the supernatant of the suspension in the absence of polymer at 40°C. The solid curve was obtained with the DLVO theory by using κ^{-1}= 2.0 nm and A= 2.20×10^{-20} J and a fitted potential of -33 mV. The inset shows the normalized adhesion force distribution. 75

Figure 5.8 Long-range interaction and adhesion forces in the supernatant of the suspension in the presence of 500 ppm polymer. The inset shows the adhesion force distribution. 77

Figure 5.9 Typical retraction force profile recorded between two kaolinite particles in the supernatant of the suspension in the presence of 200 ppm polymer at 40°C. 77

Figure 5.10 Initial settling rates as a function of adhesion forces between two kaolinite particles. 78

Figure 6.1 Bitumen recovery at various polymer dosages using extraction procedure I. 81

Figure 6.2 Bitumen froth quality (B/S and B/W) at various polymer dosages at room temperature. 81

Figure 6.3 Settling curves of oil sands tailings at various polymer dosages at room temperature. 82

Figure 6.4 Bitumen recovery at various polymer dosages using extraction procedure II (i.e. bitumen flotation was conducted at 40°C). 85

Figure 6.5 Bitumen froth quality (B/S and B/W) at various polymer dosages at 40°C. 86

Figure 6.6 Settling curves of oil sands tailings at various polymer dosages at 40°C. 87

Figure 6.7 Initial settling rate of oil sands tailings as a function of polymer dosage at 40°C. 88

Figure 6.8 A photo showing tailings settling at various polymer dosages at 40°C. 88

LIST OF TABLES

Table 3-1 Chemicals used in the synthesis of Poly(NIPAM) 25

Table 5-1 Inorganic components of Aurora process water 64

NOMENCLATURE

A	Hamaker constant, J
A_{132}	Hamaker constant of phase 1 and phase 2 through a medium 3, J
a	spherical particle radius, m
c	concentration of a polymer solution, g l^{-1}
C	electrolyte concentration, M
C_0, C_1, C_2	constants for evaluation of hydrophobic force, N m^{-1}
F_{total}	sum of all interaction forces, N
F_E	electrostatic double layer force, N
F_{HB}	hydrophobic force, N
F_S	steric force, N
F_V	van der Waals forces, N
h	separation distance between two surfaces, m
k	Boltzmann constant, 1.381×10^{-23} J K^{-1}
L	length of polymer tail, m
$\overline{M_n}$	number average molecular weight, dimensionless
N_B	number of monomer units per polymer chain, dimensionless
n_j	number density of ions j in the solution, m^{-3}
$n_{j\infty}$	number density of ion j in the bulk solution, m^{-3}
R	radius of a spherical particle, m
s	average spacing between two grafted points of polymer molecules
T	absolute temperature, K

U_E	electrophoretic mobility, $(m\ s^{-1})/(V\ m^{-1})$
z_j	valence of ion j in solution
η	viscosity of a polymer solution, $m^2\ s^{-1}$
η_0	viscosity of pure solvent, $m^2\ s^{-1}$
η_{sp}	specific viscosity, dimensionless
$[\eta]$	intrinsic viscosity of a polymer, $mL\ g^{-1}$
Ψ	potential in an electric double layer, V
ρ	gravity density, $Kg\ m^{-3}$
κ^{-1}	Debye length, m
ε	relative permittivity of a medium, dimensionless
ε_o	permitivity of vacuum, $8.854\times 10^{-12}\ C\ V^{-1}\ m^{-1}$
∇^2	Laplacian operator, m^{-2}
γ	interfacial energy, $J\ m^{-2}$

Chapter 1 Introduction

Oil sands, also known as tar sands or bituminous sands, are a complex mixture of bitumen, sands, water and clays. The amount of bitumen in oil sands varies from 0-16% by weight. A typical oil sands ore from a commercial open-pit mining operation usually contains about 9-12% bitumen by weight. Currently, water-based processes based on Clark Hot Water Extraction (CHWE) technology (Clark and Pasternack, 1932), are used to extract bitumen from oil sands.

Figure 1.1 shows a schematic flow diagram of a typical oil sands extraction process. The process mainly includes the following units: mining, extraction, froth treatment and tailings management. Oil sands ore is first mined and mixed with water and additives to form oil sands slurry from which bitumen is liberated and recovered by flotation. The recovered bitumen froth is treated further in froth treatment unit, and the produced tailing slurry after bitumen extraction is discharged into tailings ponds for solid-liquid separation. Coagulants or flocculants are usually added to accelerate the tailings settling. The released water from tailings ponds is then recycled back to the extraction plant for reuse.

In the extraction process, caustic is often added to improve bitumen extraction (Sanford and Seyer, 1978; Misra et al., 1981; Sanford, 1983). However, the addition of caustic led to a high slurry pH which would result in a slow tailings settling (Sanford and Seyer, 1979; Smith and Ng, 1993). In the tailings treatment, gypsum is used as a coagulant to accelerate the settling of fine solids in the tailings slurry (Matthews et al.,

2002) while the calcium remained in the recycle water can impose a detrimental impact on bitumen recovery (Zhou et al., 1999; Basu et al., 2003).

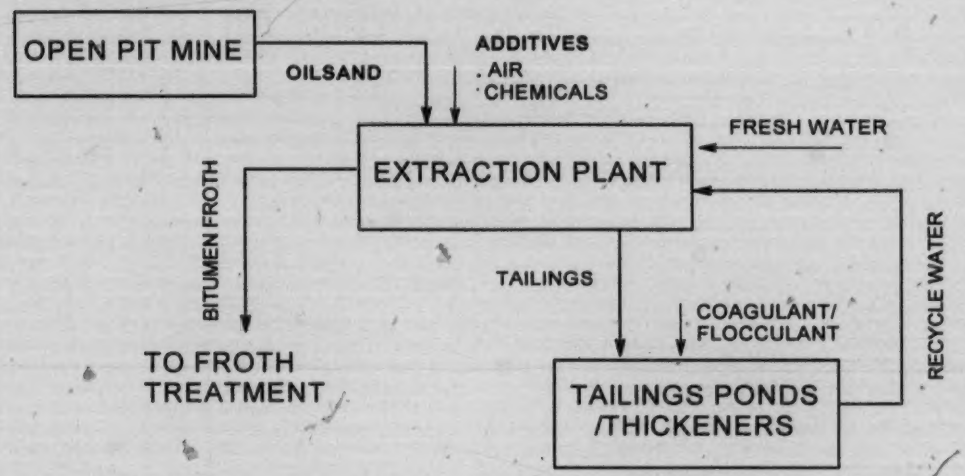

Figure 1.1 Simplified flow diagram of an oil sands extraction process.

It is desirable to design a chemical which can improve bitumen recovery as well as the tailings settling. In this study, a temperature-sensitive polymer, poly(N-isopropylacrylamide), was synthesized and used in oil sands extraction and tailings treatment. The main purpose of this thesis was to study the role of the polymer as a process aid in oil sands extraction and as a flocculant in tailings treatment. The first task is to synthesize the polymer having a high molecular weight. Free radical polymerization was used. The second task is to treat the prepared clay suspensions using the polymer following two different settling procedures. To illustrate the role of the polymer in the flocculation of clay suspensions, the colloidal forces between two clay particles were measured using an atomic force microscope in the presence of the

polymer. The measured forces correlate with the settling results. The final objective is to study the effect of the polymer as a process aid on low-grade oil sands processing.

The organization of this thesis is as follows.

Chapter one gives a brief introduction to oil sands extraction and tailings treatment, and the objectives and organization of the thesis.

Chapter two reviews the literature of oil sands processibility, tailings treatment methodology, and colloidal forces between fine clays.

In chapter three, experimental procedures, including polymer preparation, clay suspensions settling, oil sands extraction, zeta potential distribution measurement, and surface force measurement, are described.

Chapter four presents the results of the polymer as a flocculant in a model system: kaolinite clays in de-ionized water. The settling results and measured surface forces between two kaolinite particles are qualitatively reported.

Chapter five demonstrates the flocculation performance of the polymer in a practical system: kaolinite clays in Aurora plant process water. The settling results and measured AFM forces are given to explain the flocculation performance of the polymer.

Chapter six concerned about the roles of the polymer as a process aid to treat low-grade oil sands ore. Effects of the polymer on bitumen recovery, froth quality, and tailings settling following two different extraction procedures are discussed.

The general conclusions are given in chapter seven.

Chapter 2 Literature review

2.1 Current methodology of oil sands tailings management

In a water-based extraction process, a large amount of water is used in bitumen extraction, producing a large volume of tailings. It has been estimated that for every 1 m^3 of bitumen extracted, 3 m^3 of water are used and 4 m^3 of tailings are produced. The produced tailings slurry is discharged into tailings pond for solid-liquid separation. Due to very slow settling of fine solids in the tailings ponds, there is a large accumulation of fine tailings. It is estimated that the volume of the mature fine tailings (MFT), an aged aqueous suspension of fines, will increase to over one billion cubic meters by year 2020 (Chalaturnyk et al., 2002). As a large volume of water is used in bitumen extraction, to reduce the usage of fresh water from Athabasca river, the water released from tailings ponds is usually reused. Therefore, a sustainable development of oil sands industry relies largely on the development of solutions for water reuse and tailings management.

In tailings treatment, as shown by Figure 2.1, course solids first settle out to form the dyke and beach, while the fines and residual bitumen are carried into the pond where Stokian and hindered settling take place. Over years, three zones are formed in the tailings pond. On the top is the free water zone of about three meters of clear water. Beneath the top layer is a transition zone of about 1 meter thick, consisting of water and clay particles. At the bottom is the fine tailings zone, a layer of clays, fine sands, residual bitumen and water (Sethi, 1993). The fine tailings contain high concentration of ultra-fines and organic compounds such as naphthenic acids and hydrocarbons. The ultra-fine particles settle extremely slowly. After several years, a stable suspension

would be formed, causing an environmental liability to the industry. Some researchers attributed the extremely slow settling of the fine tailings to the dispersing nature of the ultra-fine particles as well as the water chemistry of the fine tailings (Xu and Hamza, 2003; Xu et al., 2004). Others (Mikula et al., 1993) considered that the high water-holding capacity of the fine tailings was attributed to the three-dimensional gel structure formed over the years. In fine tailings, the fine particles are not individually suspended but are in an aggregated state. Over years, the formed small flocs interfere with each other, forming a three-dimensional gel network structure. Other components, such as coarser solids and free bitumen, are trapped into this network during its formation.

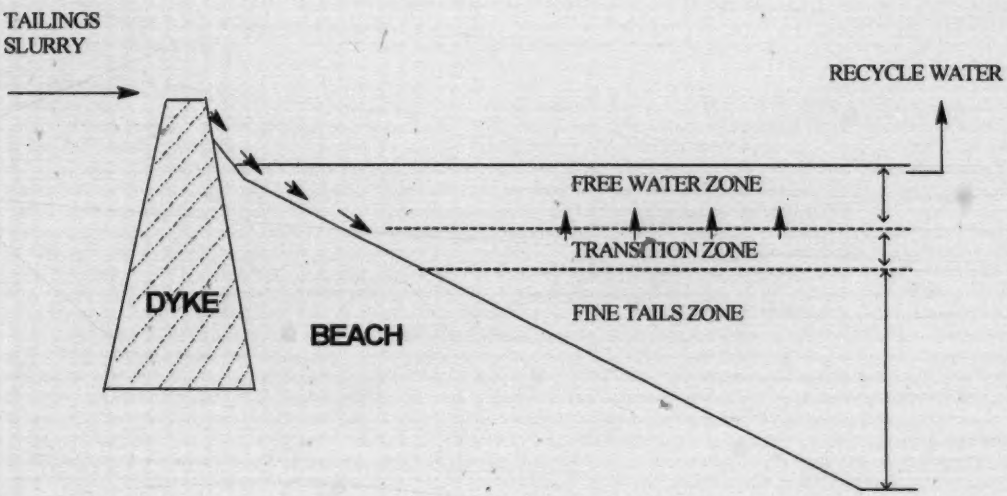

Figure 2.1 Cross section of an oil sands tailings settling basis.

Considerable efforts have been made in the past to develop suitable technologies to reduce the inventories of the fine tailings. Several processes were developed, including the composite tailings (CT) process (Matthews et al., 2002) and the paste technology (Xu and Hamza, 2003; Xu et al., 2004). In the CT process, an inorganic coagulant and coarse sands are added to the MFT to cause a quick release of process water for recycle. Different coagulants were tested to treat the MFT, including acids, lime, gypsum, and alum. Sulphuric acid was able to produce nonsegregating sediments of the fine tailings (Mackinnon et al., 2001), but changed the pH level and ionic contents of the released water. Lime and gypsum were also effective to produce nonsegregating sediments of the fine tailings (Caughill et al., 1[illegible] Matthews et al., 2002). However, their use resulted in a high concentration of free calcium cation in the recycle water, which was found to be detrimental to bitumen extraction (Hepler and Smith, 1994; Kasongo et al., 2000).

Although inorganic coagulants can achieve a good tailings settling, the increased salinity in the recycle water is of some concerns. Therefore, organic flocculants have been tested as an alternative to treat oil sands tailings. For example, in the paste technology organic polymers are used to thicken oil sands tailings into a paste. The flocculation performance of polymers was found to be affected by several factors, including the molecular weight, charge density, polymer concentration, and electrolytes in aqueous solutions. Klimpel (1997) found that polymers with lower molecular weights had a tendency to form small but tighter flocs. On the contrary, polymers with high molecular weights formed larger but looser flocs. Abraham et al. (2004) studied the effect of the charge density of polyacrylamide-acrylic acid copolymers on the

flocculation of silica suspensions. Polymers with a high charge density led to fast flocculation while polymers with a low or medium charge density only led to a slow flocculation. Sworska et al. (2000) studied the impact of pH on the flocculation of the fine tailings using a polyacrylamide flocculant. At a low pH, the addition of an anionic polyacrylamide led to a high quality of the supernatant, i.e. a low solid content in the supernatant. In an alkaline pH, the polymer led to a poor supernatant quality, i.e. a high solid content in the supernatant. Sworska et al. (2000) also found that the presence of divalent cations with the polymer addition exhibited a synergetic effect on tailings settling. It led to a fast settling as well as a high quality of the supernatant. This finding was verified by Long et al. (2006). They measured the adhesion forces between fine solids using an atomic force microscope (AFM). The presence of both the polymer and calcium (or magnesium) significantly increased the adhesion force between fine solids. The molecular structure of polymers also exhibited a great impact on the flocculation and dewatering behavior. For example, non-ionic polyethylene (PEO) produced better inter-particle bridging than anionic polyacrylamide-acrylate copolymer, resulting in a faster settling and more compacted flocs (Mpofu et al., 2004a; 2004b).

2.2 Temperature-sensitive polymer flocculants

In the paste technology, polyacrylamides or its derivatives are used to treat oil sands tailings. The formed flocs by polyacrylamides are usually loose and trap a large amount of water, which is very difficult to release (Igarashi and Sakohara, 2001). It is desirable to design a polymer flocculant which can form more compacted flocs. Recently, temperature-sensitive polymers were found to be able to form much denser

flocs than polyacrylamides (Igarashi and Sakohara, 2001). Temperature-sensitive polymers exhibit a thermally reversible soluble-insoluble change in aqueous solutions with temperature across their phase transition temperatures (PTT). Figure 2.2 illustrates the molecular structure change of a temperature-sensitive polymer with temperature. When temperature is below its PTT, the polymer has a long extended structure. It is hydrophilic and soluble in aqueous solutions (Heskins and Guillet, 1968; Schild, 1992). When temperature is above its PTT, the polymer is of a coiled conformation. It becomes hydrophobic and insoluble in aqueous solutions.

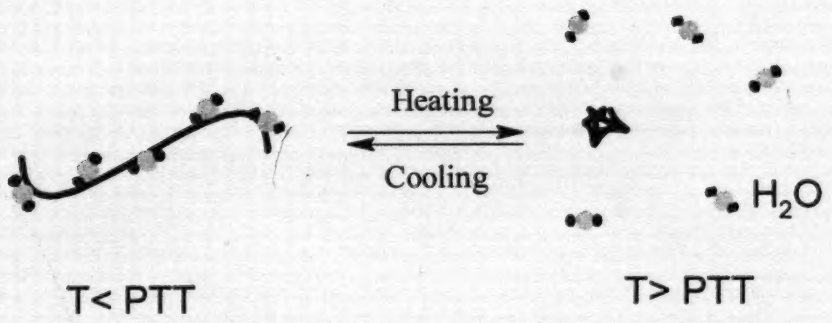

Figure 2.2 Schematic illustration of the structure change of a temperature sensitive polymer with temperature.

Poly *N*-isopropylacrylamide (Poly(NIPAM)) is a representative nonionic temperature-sensitive polymer, which has a phase transition temperature of about 32°C (Heskins and Guillet, 1968). Poly(NIPAM) is extensively studied because of its relatively sharp transition temperature (Wu et al., 2003). Figure 2.3 shows the chemical structure of poly(NIPAM). Two functional groups, acrylamide and isopropyl groups,

are contained in the polymer chain. Below the phase transition temperature, acrylamide groups hydrate, resulting in an extended chain structure in an aqueous solution (Ramon et al., 2001; Katsumoto et al., 2004). When temperature is above the phase transition temperature, isopropyl groups dehydrate, leading to a compacted conformation. Chiaki et al. (2001) studied the effect of the hydrophobic group sizes on the phase transition temperatures. They found that the larger the hydrophobic group, the higher the phase transition temperature.

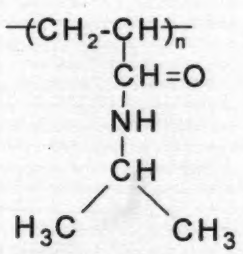

Figure 2.3 Chemical structure of poly(NIPAM)

Because of the unique characteristic of the phase transition with temperature, temperature-sensitive polymers used as flocculants for solid-liquid separation are receiving more and more attention. Dzinomwa et al. (1997) used temperature-sensitive polymers to dewater fine coal slurry and achieved a high dewatering performance. Deng et al. (1996) used a temperature-sensitive polymer, poly(N-isopropylacrylamide-co-diallyldimethylammonium chloride), to flocculate TiO_2 suspensions. They found that the copolymer induced the flocculation of TiO_2 suspensions at a temperature below or above the phase transition temperature. But the flocculation was more rapid at a

temperature above the phase transition temperature. Sakohara et al. (2004) found that a cationic temperature-sensitive copolymer of N-isopropylacrylamide and N, N-dimethylaminopropylacrylamide led to more compacted sediments of TiO_2 suspensions. Guillet et al. (1985) described flocculation of suspended particles using temperature-sensitive polymers in a patent. The main claim of their patent was that below the phase transition temperature, temperature-sensitive polymers were effective flocculants, exhibiting a behavior similar to that of polyacrylamides, whereas above the phase transition temperature, they became poor flocculants. In contrast, others (Atago et al., 1992; Sakohara et al., 2000; Sakohara and Nishikawa, 2000; Igarashi and Sakohara, 2000) found that temperature-sensitive polymers resulted in flocculation even at a temperature above their phase transition temperatures. The discrepancy may be due to the different procedures used by these investigators in the mixing and settling steps.

2.3 Oil sands processibility

2.3.1 Effect of oil sands ore grade

Oil sands ores are usually divided into high-grade or low-grade ores. Generally a high-grade ore refers to an ore with a "high" bitumen but "low" fines content. A low-grade ore refers to an ore with a "low" bitumen but "high" fines content. The fines are conventionally defined as mineral solids smaller than 44 microns. A strong correlation was observed between bitumen recovery and oil sands ore grade (Takamura and Wallace, 1987; Cuddy, 2000; Tipman, 2000). High bitumen recoveries were obtained from high-grade ores while a low bitumen recovery was obtained from a low-grade ore. The low bitumen recovery from a low grade ore is generally attributed to a high content

of fines in the ore, causing a slime coating of bitumen surface, i.e. the coating of bitumen surface by a layer of fine solids. The zeta potential distribution and AFM measurements were successfully applied to the study of slime coating phenomena (Liu, 2004; Liu et al., 2005a). In the study of Liu et al. (2005a), the zeta potential distributions of individual bitumen, fines and their mixture (1:1 ratio) were compared. The bitumen and fines used in zeta potential measurements were extracted from both high and low grade ores. For low grade ore, the zeta potential distribution of the mixture of bitumen and fines was located at the value of individual fines, indicating that the bitumen droplet was fully covered by fines. For high grade ore, no such slime coating was observed, indicating little coagulation between bitumen and fines. These findings were reinforced by the measured bitumen-fine interaction forces using an atomic force microscope (Liu et al., 2004a; 2004b; 2005b). For high grade ores, strong repulsion and weak adhesion between bitumen and fines were measured while strong attractive long-range interaction force and adhesion were observed for low grade ores.

2.3.2 Effect of water chemistry

Currently, up to 75% water used in upgraded bitumen production comes from plant process water recycled from tailings ponds. The chemistry of the recycle water has a strong impact on bitumen extraction, froth treatment and tailings treatment. Due to the addition of chemicals such as caustic and calcium sulfate in bitumen extraction process and tailings treatment, a high level of free ions remain in the process water (Baptista and Bowman, 1969; Ali, 1975; Zhao et al., 2006). These ions include sodium, calcium, magnesium, sulfate, bicarbonate, chloride, etc. The calcium and magnesium cations in the process water can cause clay particles to coat on bitumen surface (Hepler

and His, 1989; Hepler and Smith, 1994; Smith and Schramm, 1992; Kasongo et al., 2000). The clays coated on bitumen surface set a barrier for bitumen-air bubble attachment, leading to a low flotation efficiency and hence a low bitumen recovery. Liu et al. (2004a) also studied the effect of calcium cations on the interaction between bitumen and montmorillonite clay in a 1mM KCl solution. In the presence of calcium cations, the electrical double layer force between bitumen and montmorillonite was depressed and a strong adhesion force was observed, indicating a strong attachment of montmollinite clay on the bitumen surface. However, calcium cations were found to increase the settling and supernatant quality of the tailings (Sworska et al., 2000; Richard et al., 2002; Masliyah et al., 2005). Due to a high concentration of sodium ions present in the process water, the effect of sodium ions on bitumen recovery was studied by several researchers (Takamura and Wallace, 1987; 1988; Hepler and Smith, 1994). A low sodium concentration (e.g. below 10 mM) had little effect on bitumen recovery while a high sodium concentration (e.g. above 50 mM) induced a coagulation of bitumen and clays, thereby reducing bitumen recovery.

2.3.3 Effect of process aids

In oil sands extraction, process aids (chemicals) are widely investigated for improving the processibility of oil sands, especially for low-grade oil sands ores (Attia and Deason, 1989; Dai et al., 1992; Pradip et al., 1993; Li et al., 2005a). The chemicals studied in oil sands processing mainly include caustics, dispersants, surfactants and organic polymers. The addition of caustic at an optimal dosage increased bitumen recovery and froth quality (Clark and Pasternack, 1932; Sanford, 1983). But it also caused a high pH level and free surfactants release, leading to a slow settling and high

toxicity of oil sands tailings (Speight and Moschopedis, 1978; Smith and Ng, 1993; Schramm et al., 2000). Silicates or phosphates as dispersants were also tested in oil sands processing. Li et al. (2005a) found that acidified silicates led to a higher degree of bitumen liberation from sand grains, a faster bitumen flotation rate, and a better bitumen froth quality than caustic addition.

Although the addition of inorganic aids can improve bitumen recovery, they can cause problems in tailings treatment as well. Organic polymers as an alternate were therefore tested in oil sands processing. Li et al. (2005b) studied the effect of hydrolyzed polyacrylamide on low-grade oil sands processing. The addition of the polymer at an appropriate dosage not only improved bitumen recovery but also increased the tailings settling because of the selective flocculation of fines by the polymer. Polymeric dispersants such as polyethylene oxide (PEO), polyvinyl pyrrolidone (PVP), were also tested as flocculants for clay fines to control slime coating (Attia and Deason, 1989; Pradip et al., 1993).

2.4 Surface force review

Bitumen liberation, flotation or clay fines flocculation can be best understood within the framework of electrokinetic, interfacial and fluid particle dynamics theories. For example, the flocculation of clay fines is controlled by the interaction between clay fines and by the interfacial properties of the clay surfaces.

Particulates, such as clays or mineral solids suspended in an aqueous solution, are subjected to various forces that determine the nature of interactions between the

particles. The overall interaction determines whether a clay particle would attach to other fines.

2.4.1 Electrokinetics

A surface immersed in an electrolyte solution is usually charged due to specific adsorption of ions, dissociation of surface species or crystal lattice defect (Hunter, 1993; Warszynski et al., 1997). The surface charges can be balanced by counter-ions to form an electric double layer. Figure 2.4 shows an electric double layer model developed by Stern (1924) and Grahame (1947). The counter-ions bound to the surface form the *Stern layer* while the remaining counter-ions form a diffuse mobile cloud in rapid thermal motion, and extending out from the surface. The boundary of one to two radii of ions away from the surface is referred to the shear plane. The potential at shear plane is called zeta potential.

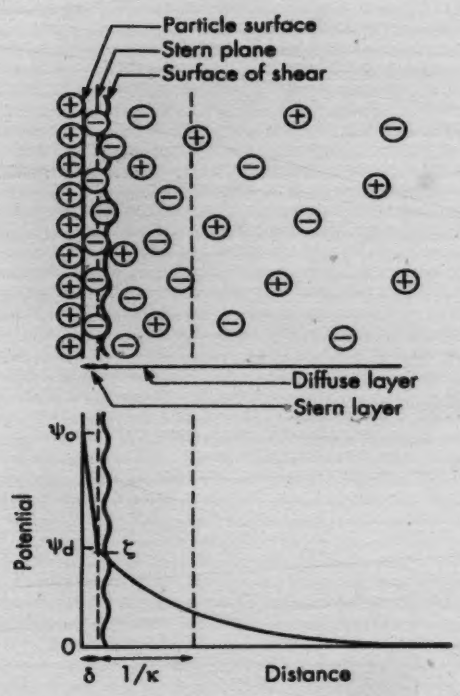

Figure 2.4 Schematic of Stern double layer model.

The distribution of electrolyte ions within the diffuse double layer obeys Boltzmann distribution (Israelachvili, 1992):

$$n_j = n_{j\infty} \exp(\frac{-z_j e \psi}{kT}) \qquad (2\text{-}1)$$

where n_j is the number density of ions j with valence z_j, $n_{j\infty}$ is the number density of ions j in the bulk, ψ is the electrical potential in the double layer, e is the electron charge, k is Boltzmann constant, and T is absolute temperature.

From Boltzmann distribution, we can obtain the non-linear Possion-Boltzmann equation as:

$$\varepsilon\varepsilon_0\nabla^2\psi = -e\sum_j z_j n_{j\infty} e^{-\frac{z_j e\psi}{kT}} \qquad (2\text{-}2)$$

If the surface potential (ψ) is small, Debye-Hückel approximation can be applied to the non-linear Possion-Boltzmann equation (Israelachvili, 1992). The Debye length (κ^{-1}) is then obtained as

$$\kappa^{-1} = \left(\frac{\varepsilon\varepsilon_0 kT}{\sum_j n_{j\infty} e^2 z_j^2} \right)^{1/2} \qquad (2\text{-}3)$$

κ^{-1} is a characteristic parameter describing the double layer thickness or the decay of the electric potential, and therefore determining the electrostatic interactions between the two surfaces.

2.4.2 Long-range force

2.4.2.1 Electric double layer force

When two surfaces approach each other, a repulsion or attraction force would exist between the two surfaces because of the overlap of their electric double layers. The general expression for the interaction potential energy of two unequal spheres of radii R_1 and R_2 having surface potentials ψ_1 and ψ_2 was given by Hogg et al. (1966) as

$$V_R(h) = \frac{\pi\varepsilon R_1 R_2}{R_1 + R_2}\left\{2\psi_1\psi_2 \ln\left[\frac{1+\exp(-\kappa h)}{1-\exp(-\kappa h)}\right] + (\psi_1^2 + \psi_2^2)\ln[1-\exp(-2\kappa h)]\right\} \quad (2\text{-}4)$$

White (1983) generalized Derjaguin approximation (Derjaguin, 1934) to evaluate the interaction energy between two curves of surfaces. In this approximation, the total interaction energy of two spheres of radii R_1 and R_2 is given by the Derjaguin approximation as

$$V_R(h) = \frac{4\pi\varepsilon R_1 R_2 \psi_s^2}{R_1 + R_2}\int_h^\infty \frac{\exp(-k x)dx}{1+\exp(-\kappa x)} \quad (2\text{-}5)$$

where, R_1 and R_2 are spherical particle radius, ε is dielectric constant of the media, κ is the reverse Debye length, ψ_s is surface potential, h is the separation distance.

2.4.2.2 Van der Waals forces

Due to the molecular interaction, similar particles are attracted to each other. This force is called van der Waals force. For a system of two spheres, it is given as equation (2-7) (Masliyah, 1994). It usually dominates over a range of 0.2-10 nm, and is influenced by the presence of electrolyte solution and the type of particles.

$$\frac{F_v}{R} = -\frac{A}{6h^2} \quad (2\text{-}6)$$

$$R = \frac{R_1 R_2}{R_1 + R_2} \quad (2\text{-}7)$$

where, A is Hamaker constant, h is the separation distance, R_1 and R_2 are spherical particle radius. Usually, the Hamaker constant (A) for a given material can be calculated as (Israelachvili, 1992):

$$A = \frac{3}{4} kT \left(\frac{\varepsilon - 1}{\varepsilon + 1} \right)^2 + \frac{3h\nu_e}{16\sqrt{2}} \frac{(n^2 - 1)^2}{(n^2 + 1)^{3/2}} \qquad (2\text{-}8)$$

where, ε is the static dielectric constant, n is the refractive index of the medium in the visible region, and ν_e is the main electronic absorption frequency of material in the UV-visible region (typically around 3×10^{15} s^{-1}).

Hamaker constants for a given system can also estimated by:

$$A_{132} = (\sqrt{A_{11}} - \sqrt{A_{33}})(\sqrt{A_{22}} - \sqrt{A_{33}}) \qquad (2\text{-}9)$$

where A_{ii} is the known Hamaker constant of material i, and 3 often is referred to as medium

2.4.2.3 Steric force

Steric forces are often found in systems involving brush-like surfaces such as polymer-covered surfaces. When two polymer-covered surfaces approach each other, they experience a force once their outer segments begin to overlap. This interaction usually leads to a repulsive osmotic force due to the unfavorable conformation associated with compressing the polymer chains between the surfaces (Israelachvili, 1992). Theories of steric interactions are complex, depending on the coverage of polymer on each surface, on whether the polymer is simply adsorbed from solution (i.e.

a reversible process) or irreversibly grafted onto the surfaces, or/and on the quality of the solvent. *de Gennes* (1987) proposed a model to calculate steric forces for uncharged polymeric surfaces:

$$\frac{F_S}{R} = \frac{16\pi kTL}{35s^3}\left[7\left(\frac{h}{2L}\right)^{-5/4} + 5\left(\frac{h}{2L}\right)^{7/4} - 12\right] \qquad (2\text{-}10)$$

where L is the thickness of polymeric layer, s is the average spacing between two grafted points of polymer molecules, and h is the separation distance between a sphere and plate. For the surfaces covered by charged polymers, Pincus (1991) developed an expression of steric forces as:

$$\frac{F_S}{R} = \frac{4\pi kTN_B^2}{Cs^4}\left[\frac{1}{h} - \frac{1}{2L}\right] \qquad (2\text{-}11)$$

where C is the salt concentration, and N_B is the number of monomer units per chain.

2.4.2.4 Hydrophobic force

Between two hydrophobic surfaces exists a long-range attractive hydrophobic force (F_{HB}). It typically extends to a separation distance of 20 nm or in some cases to over 100 nm (Škvarla, 2001). Several empirical relationships were proposed to calculate this force (Israelachvili and Pashley, 1984; Claesson et al., 1986, Rabinovich and Yoon, 1994; Graig et al., 1999). These expressions are listed as equations from (2-12) to (2-14).

$$\frac{F_{HB}}{R} = -C_0 \exp(-\frac{h}{h_0}) \qquad (2\text{-}12)$$

$$\frac{F_{HB}}{R} = -C_1 \exp(-\frac{h}{h_1}) - C_2 \exp(-\frac{h}{h_2}) \quad (2\text{-}13)$$

$$\frac{F_{HB}}{R} = -\frac{K}{6h^2} \quad (2\text{-}14)$$

where, h is the separation of two surfaces, C_0, C_1, C_2, h_0, h_1, h_2 and K are empirical constants which depend on the hydrophobicity of the surfaces.

2.4.2.5 DLVO theory

The colloidal interaction forces are generally elucidated by the DLVO (Derjaguin, Landau, Verwy, and Overbeek) theory. The classical DLVO theory includes attractive van der Waals interaction force (F_V) and electrostatic double layer repulsion (F_E) (Israelachvili, 1992), expressed as:

$$F_{total} = F_V(A, R, h) + F_E(\psi_s, R, \kappa, h) \quad (2\text{-}15)$$

In cases of other forces, the total force can be expressed as equation (2-16), called extended DLVO theory:

$$F_{total} = F_E + F_V + F_{HB} + F_S + \ldots \quad (2\text{-}16)$$

where F_E is the electrostatic double layer force; F_V is van der Waals forces; F_{HB} is hydrophobic force; F_S is steric force.

2.4.3 Contact adhesion force

It is important to understand interparticle adhesion forces as applied to many processes such as mineral separation and particle coagulation or flocculation in colloidal dispersions. The adhesion forces between two surfaces mainly originate from the molecular/atomic interactions in the contact area, such as electrostatic interaction, chemical bond and hydrogen bonding.

2.4.3.1 Work of adhesion

Work of adhesion is the free energy change to separate unit areas of two surfaces 1 and 2 from contact to infinity. In the case of separating two surfaces 1 and 2 in medium 3, the energy change can be expressed as (Israelachvili, 1992)

$$W_{132}=W_{12}+W_{33}-W_{13}-W_{23}=\gamma_{13}+\gamma_{23}-\gamma_{12} \qquad (2\text{-}17)$$

where W_{ij} and γ_{ij} are the work and interfacial tension to separate unit areas of two surfaces i and j (i or j = 1, 2 or 3), respectively.

2.4.3.2 Adhesion force between solid particles

From Derjaguin approximation (Derjaguin, 1934), the adhesion force (F_{ad}) between two rigid macroscopic spheres can be expressed by

$$\frac{F_{ad}}{R}=2\pi W_{132} \qquad (2\text{-}18)$$

where, $R=(R_1R_2)/(R_1+R_2)$, R_1 and R_2 are the radii of spheres 1 and 2, respectively, W_{132} is the work of adhesion. However, real particles are never completely rigid. They

deform elastically under the influence of any externally applied load as well as the attractive inter-surface forces that pull the two surfaces together. This gives rise to a finite contact area even under zero external loads. Johnson, Kendall and Roberts (1971) proposed a theory (JKR theory) to provide a rigorous theoretical treatment of the adhesion of elastic spheres. In the JKR theory, the radius of contact area of two spheres can be expressed as equation (2-19), and the adhesion force is given as (2-20):

$$a = \left(\frac{R}{K} \left(F + 3\pi\gamma R + \sqrt{6\pi\gamma RF + (3\pi\gamma R)^2} \right) \right)^{1/3} \tag{2-19}$$

$$\frac{F_{ad}}{R} = \frac{3}{2}\pi\gamma \tag{2-20}$$

where, γ is interfacial energy (Jm^{-2}), K is elastic moduli, W_{12} is surface energy per unit area, and F is external load.

Derjaguin, Muller and Toporov (1975) also proposed a theory (DMT theory) to calculate the adhesion force induced by the contact deformation. The expression of radius of contact areas (a) and adhesion force are given in equation (2-21) and (2-22), respectively. DMT theory is only applicable for rigid surfaces with a low adhesion force and a small radius.

$$a = \left(\frac{R}{K} \left(F + 2\pi\gamma R \right) \right)^{1/3} \tag{2-21}$$

$$\frac{F_{ad}}{R} = 2\pi\gamma \tag{2-22}$$

2.5 Summary of literature review

In this review, we introduced oil sands extraction process and associated tailings treatment. In oil sands extraction process, several impact factors were reviewed, including ore grade, water chemistry of slurry and process aids. Effect of process aids such as organic polymers on oil sands processing was discussed. Water chemistry of oil sands slurry was introduced as well. Because the majority of water used in oil sands extraction comes from plant process water, the effect of the components contained in plant process water on bitumen extraction and tailings treatment is also discussed.

In tailings treatment, we first introduced current methodology of oil sands tailings management, including the composite tailings (CT) and the paste technology. Polymers with high molecular weight are used to flocculate the fines in oil sands tailings. Among those polymer flocculants, temperature-sensitive polymers were reviewed because they can form dense flocs and hence cause a quick water release. In order to explain the flocculation behaviour of temperature-sensitive polymers in tailings treatment, DLVO theory is introduced. The surface forces, such as electric double-layer forces, van der Waals forces, steric forces and hydrophobic forces, are discussed.

Chapter 3 Experimental procedures

3.1 Polymer preparation

PolyN-isopropylacrylamide, a representative of temperature-sensitive polymers, was synthesized by free radical polymerization following procedures described in literature (Heskins et al., 1968; Guillet et al., 1985). The monomer, N-isopropylacrylamide, was obtained from Fisher Scientific. The initiator and accelerator used in the polymerization were potassium persulphate (99.99%, Sigma-Aldrich) and potassium bisulphate (>99%, Sigma-Aldrich), respectively. A list of chemicals used in the synthesis of poly(NIPAM) is given in Table 3-1. More specially, a 100 g/l N-isopropylacrylamide solution was prepared using de-ionized water. 200 ml of the prepared solution were fed into a 250 ml reactor with a stirrer, a gas inlet and outlet. The reactor was degassed by continuous purging with high purity nitrogen for one hour. While stirring, 4 ml of 5.0 g/l potassium bisulphate were added to the solution followed by the addition of 8 ml of 5.0 g/l potassium persulphate. The polymerization proceeded at room temperature for two days. After the polymerization, the mixture was first diluted with 500 ml de-ionized water. The diluted solution was left without disturbance for two days. The solution was then heated to 50°C at which the polymer became insoluble and formed precipitates. The precipitated polymer was separated from the solution by filtration. The polymer retained as filter cake was purified again by re-dissolving in de-ionized water at room temperature, heating to 50°C, and then filtration following the same procedure described above. This purification process was repeated three times. At last, the collected filter cake was then placed in a vacuum oven at 60°C

and 0.3 kPa for one day to evaporate the entrapped water to obtain the final polymer product prior to its use. A 5 g/l poly(NIPAM) stock solution was prepared by dissolving the prepared polymer in de-ionized water at room temperature.

Table 3-1 Chemicals used in the synthesis of Poly(NIPAM)

		Concentration
Monomer	N-isopropylacrylamide	0.1 g/ml
Initiator	Potassium persulphate	200 ppm
Accelerator	potassium bisulphate	100 ppm

3.2 Settling tests

3.2.1 Clay suspension preparation

Clay suspensions were prepared by dispersing kaolinite clays (Wards Natural Science Ltd., Ontario, Canada) to 10 wt% of solids in de-ionized water or in Aurora process water. De-ionized water was prepared with an Elix 5 followed by a Millipore-UV Plus Ultra water purification system (Millpore Inc., Canada). Aurora process water was obtained from Aurora plant of Syncrude Canada Ltd. Atomic absorption spectrometer (AAS) analysis shows that this water contained 47 ppm calcium and 15 ppm magnesium (Li et al., 2005a). The pH of the water is about 8.4.

3.2.2 Settling Procedures

Settling tests were conducted in 100 ml graduated cylinders. In this study, the following two settling procedures were used.

Procedure A– Settling at room temperature

A 100 ml clay suspension was first transferred into to a 250 ml beaker. A magnetic stirrer was used to mix the suspension at 1000 rpm for two minutes. Meanwhile, a predetermined volume of polymer solution was added. After the mixing, the suspension was carefully transferred to a 100 ml graduated cylinder. After inverting the cylinder several times, the cylinder was allowed to stand still, during which the mud-line (i.e. the volume of the concentrated suspension layer) as a function of time was recorded. The sediment volume was plotted as a function of time, which was referred to as settling curve. The settling curve allows us to determine the initial settling rate (m/h) from the slope of the initial linear portion of the curve (Cymerman et al., 1999). In this procedure, the temperature was maintained at room temperature throughout the process.

Procedure B– Settling at 40°C

In procedure B, the mixing of the polymer with a kaolinite suspension was performed at room temperature, following the same procedure described above. The suspension was then heated to 40°C using a heater while still under stirring. A thermometer was used to control the suspension temperature. When the temperature reached 40°C, the stirring was stopped and the suspension was transferred to a 100 ml graduated cylinder. A thermostatic water bath was used to keep the suspension

temperature at 40°C. The cylinder was inverted several times and left still in the water bath. The mud line as a function of time was then recorded.

3.3 Oil sands extraction

3.3.1 Materials

The oil sands ore used for bitumen extraction was a transition ore provided by Syncrude Canada Ltd. The ore consists of 8.8 wt% bitumen, 8.6 wt% connate water, and 82.6 wt% solids. The solids contain 33% fines (less than 44 μm in size). The water used was Aurora process water. The extraction experiments were conducted using a laboratory hydrotransport extraction system (LHES) (Wallwork et al., 2003; Li et al., 2005a), as shown in Figure 3.1. It consists of a pump, hydrotransport loop, circulating water bath, air injector, froth collector, and a CCD camera. The LHES was capable of simulating the commercial bitumen production conditions in hydrotransport slurry pipelines and primary separation vessels (PSV).

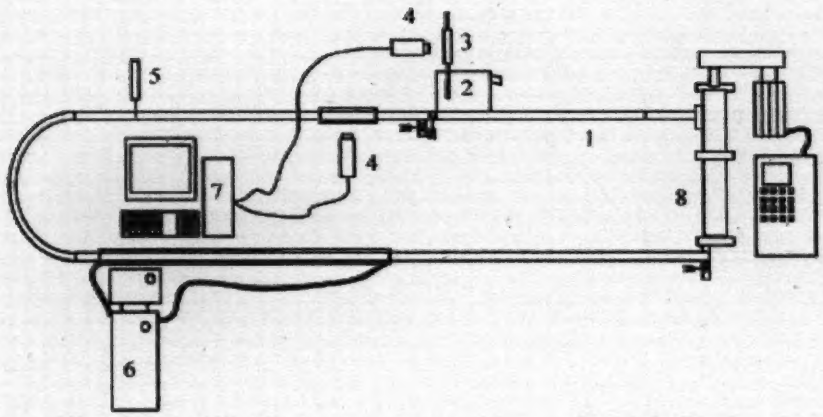

Figure 3.1 The laboratory hydrotransport extraction system (LHES). System parts: 1-Hydrotransport loop, 2-Froth collector, 3-Sample visualized tube, 4-CCD camera, 5-Air injection, 6-Circulating bath, 7-Computer, 8- Pump.

3.3.2 Extraction procedures

In bitumen extraction experiments, two procedures (I and II) similar to the settling procedures were designed in this study.

Procedure I – Both conditioning and flotation at room temperature

For each bitumen extraction experiment, 5 liters of Aurora process water with a desired amount of the polymer were added to the LHES. The polymer solution was prepared following the same method as described above. One and a half kilograms of oil sands sample were then fed to the extraction system. The formed slurry was first conditioned at room temperature by circulating the slurry at a flow rate of 3 m/s for 5 minutes. Air was then introduced into the slurry at a rate of 195 ml/min for bitumen flotation. The flotation time was recorded using a digital timer. The system was kept at

room temperature. Six froth samples were collected at different time intervals over 60 minutes. Slurry pH was not controlled during bitumen flotation. After the extraction experiment, the tailings sample was taken directly from the loop for tailings settling tests. The pH of the tailings sample was measured using a pH meter. The froth samples were then assayed using Syncrude standard procedure (Dean Stark) to determine bitumen, solids, and water content (Syncrude Analytical Methods, 1979). Bitumen recovery was calculated on the basis of the weight ratio of bitumen in the froth to that in the feed.

Procedure II – Conditioning at room temperature and flotation at 40°C

In procedure II, the oil sands slurry was first conditioned at room temperature, following the same procedure described above. After the conditioning, the slurry was quickly heated to 40°C. A circulating water bath was used to control the temperature. Then air bubbles were introduced to the slurry at a rate of 195ml/min and bitumen flotation was conducted at this higher temperature (40°C). The flotation procedure was the same as that in procedure I.

3.4 Zeta potential distribution measurements

Zeta potential distribution was measured with a Zetaphoremeter IV™ (SEPHY/CAD), as shown in Figure 3.2. It consists of a rectangular electrophoresis cell, a pair of hydrogenated Palladium electrodes, a laser-illuminator, an optical microscope and a digital video image capture (CCD camera)/viewing system. The computerized operating system allowed accurate positioning of the optical microscope view field at a

stationary layer for accurate measurement of electrophoretic mobility. The kaolinite clay suspensions with a 0.01~0.1 wt% concentration in 1 mM KCl solution or Aurora process water were prepared in an ultrasonic bath. After settling for about 0.5 hour, the upper portion of the suspension was taken for zeta potential measurement. The prepared suspension was then used to fill to the electrophoresis quartz cell with great care of avoiding generation/trapping of air bubbles. Through the laser-illuminating and video-viewing system, the movement of the particles in the stationary layer was traced, 5 times for each direction by alternating positive/negative electrode potentials. The captured images were then analyzed by built-in imaging processing software. The measurement was conducted at room temperature. Each test was repeated for several times and the average value was reported. The measurement error was generally less than 5%.

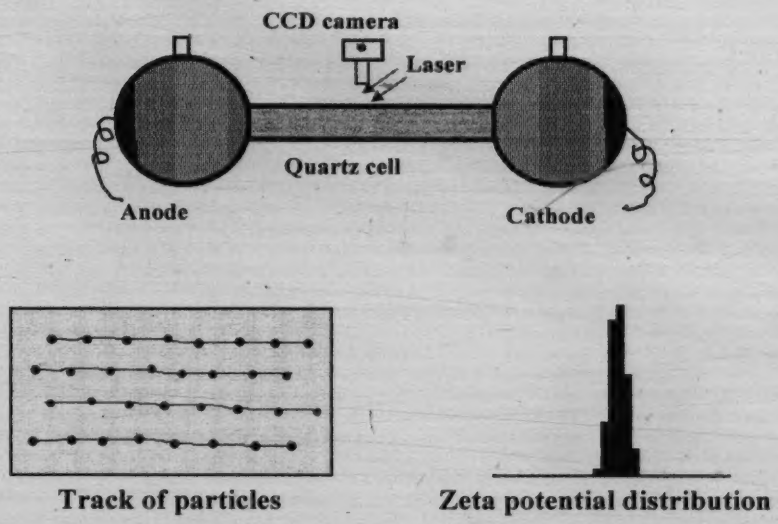

Figure 3.2 Schematic of zeta potential distribution measurement.

3.5 Surface force measurements

3.5.1 Clay probe preparation

Kaolinite particles with a pseudo spherical shape were selected as the probes for the colloidal force measurements. The particles were chosen from a great number of kaolinite particles under an optical microscope. The chosen kaolinite particle was glued onto the tip of an AFM cantilever (lever type 100 μm wide) with a spring constant of 0.58 N/m using a two-component epoxy (EP2LV, Master Bound, Hacken-sack, NJ). The glued clay probes, such as the one shown in Figure 3.3a, were allowed to set in a vacuum desiccator for more than 24 hours. Prior to each set of force measurements, the prepared probes were thoroughly rinsed with de-ionized water and ethanol followed by blow-drying with an ultra pure-grade nitrogen. The probes were then exposed to an ultraviolet light (115V, 60Hz, 0.48A, Model SP-1, UVP, USA) for more than 5 hours to remove any possible organic contaminants. The exact size of the kaolinite clay particle used in each set of experiments was determined with an optical microscope before the force measurements. More details on colloid probe preparation are provided elsewhere (Liu et al., 2001; Liu et al., 2003).

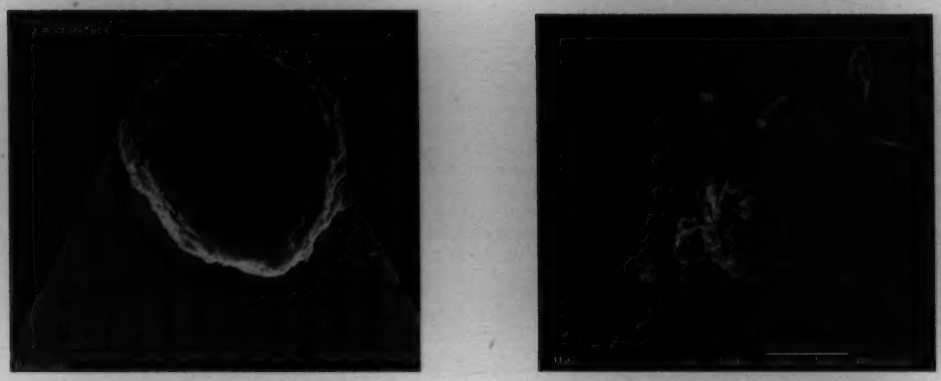

(a) (b)

Figure 3.3 (a) Kaolinite clay particle probe; (b) Kaolinite clay particles glued on a flat substrate.

3.5.2 Substrate preparation

Kaolinite particles were glued onto silica wafers of 12×12 mm^2. As in probe preparation, only a very small amount of the two-component epoxy was used under an optical microscope. To dry the glue, the prepared substrates were placed in a vacuum desiccator for one day. The prepared substrate was cleaned following the same procedure described in the section of 3.5.1. Figure 3.3b shows glued kaolinite particles on a flat substrate.

3.5.3 Surface force measurements

Surface force measurements were conducted using a Nanoscope E AFM (Digital Instruments, Santa Barbara, CA) with a vender-supplied fluid cell. A prepared substrate was mounted on the piezoelectric translation stage. A clay probe was mounted in the fluid cell. In order to position the kaolinite probe just over a kaolinite particle on the

substrate surface, an optical viewing and positioning system (Digital Instrument) was used. In our experiments, a prepared solution was slowly injected into the fluid cell with great care to avoid the trapping of air bubbles. The system was allowed to incubate for one hour at room temperature prior to the first approach of the probe to the substrate. In the force measurements, the piezoelectric translation stage brought the substrate with kaolinite particles to approach or retract from the probe particle in the vertical (Z) direction. The forces between the probe and a particle on the substrate surface were determined from the deflection of the cantilever using Hooke's low. Each force plot represents a complete extension/retraction cycle of the piezo. When the substrate approached the probe, the long-range interaction between the two particles was measured while the adhesion (or pull-off) force between them was obtained during the retraction process after contact was made. For the force measurements conducted at 40°C, a heater and a thermometer (Digital Instrument) were used to control the temperature in the fluid cell. As the kaolinite clay particles were irregular, each experiment was repeated with three different kaolinite probes to obtain representative results. For quantitative comparison, the measured long-ranged interaction force (F) and adhesion force were normalized by the probe radius (R). More detailed description on colloidal force measurement using AFM can be found elsewhere (Ducker et al., 1992; Rabinovich et al., 1994; Liu et al., 2004a).

3.6 Summary

1. The polymerization procedure of poly(NIPAM) was introduced.

2. Two different settling procedures (Procedures A and B) and two extraction procedures (Procedures I and II) were designed for the prepared temperature-sensitive polymer, respectively.

3. The method of surface force measurement between two clay particles was described.

Chapter 4 Model system: kaolinite clays in de-ionized water

4.1 Molecular weight of poly(NIPAM)

The molecular weight of poly(NIPAM) was estimated by measuring the viscosity of a series of the polymer-in-tetrahydrofuran solutions at 27°C using a Ubbelohde viscometer (Fisher Scientific). The viscosity of a polymer solution varies with polymer concentration according to the following equation (Stuart, 2002),

$$[\eta] = \lim_{c \to 0} [(\eta - \eta_0)/\eta_0 c] = \lim_{c \to 0} (\eta_{sp}/c) \qquad (4\text{-}1)$$

where, η is the viscosity of a polymer solution of concentration c in g/l, η_0 the viscosity of pure solvent, and $[\eta]$ the intrinsic viscosity. The value of intrinsic viscosity, $[\eta]$, may be experimentally determined from the y-intercept by plotting the reduced viscosity (η_{sp}/c) as a function of the concentration of polymer solutions.

Figure 4.1 shows the results of the reduced viscosity as a function of the polymer concentration in tetrahydrofuran. A good linear relationship was obtained. From the y-intercept as indicated by the arrow in the figure, the intrinsic viscosity, $[\eta]$, was found to be 162 ml/g. The number average molecular weight, $\overline{M_n}$, is related to intrinsic viscosity of polymer by (Fujishige, 1987),

$$[\eta] = 9.59 \times 10^{-3} \overline{M_n}^{0.65} \qquad (4\text{-}2)$$

From this equation, the number average molecular weight of the polymer was calculated to be 3.2 millions. Polymers with such an average molecular weight are

suitable as a flocculant. The details of the method to measure the molecular weight of poly(NIPAM) can be found elsewhere (Fujishige, 1987; Sakohara and Nishikawa, 2000).

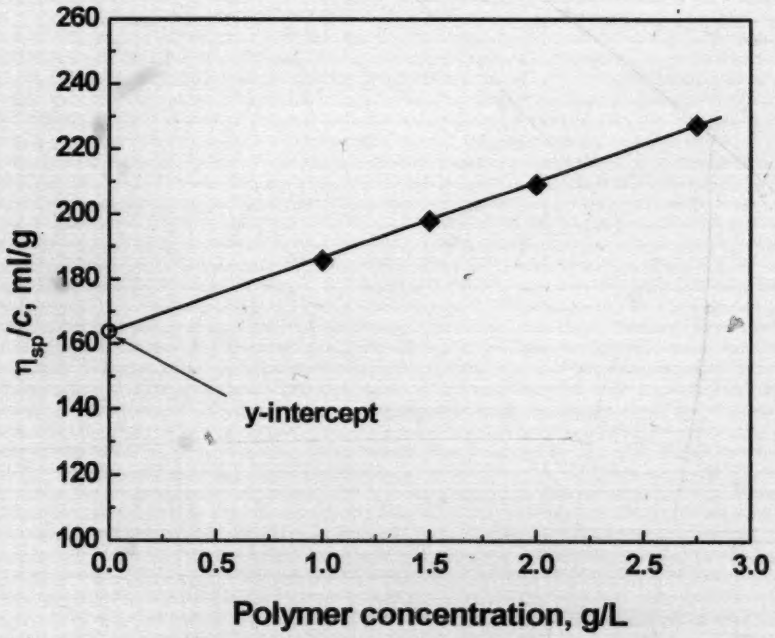

Figure 4.1 Relationship between η_{sp}/c and polymer concentration in tetrahydrofuran.

4.2 Settling of clay suspensions prepared in de-ionized water

4.2.1 Settling results

4.2.1.1 Results from procedure A

Figure 4.2 shows the effect of poly(NIPAM) addition on the settling of 10 wt% kaolinite suspensions using procedure A (i.e. both mixing and settling at room temperature). The settling curves are shown in Figure 4.2a. Figure 4.2b shows the initial settling rate as a function of polymer dosage. In the range of 0~50 ppm, the initial settling rate increased from 0.01 to 0.05 m/h. Above this dosage level, the initial settling rate decreased with further increasing the polymer dosage. When the poly(NIPAM) dosage was at 200 ppm, the initial settling rate became nearly zero. In this case, the kaolinite suspension was well dispersed by the polymer. Figure 4.2c shows that when the poly(NIPAM) dosage was increased from 0 to 50 ppm, the sediment volume after a settling period of 120 minutes decreased from 92 to 75 ml. A further increase in the polymer dosage caused an increase in the sediment volume. At the optimal polymer dosage (i.e. 50 ppm), the surface of kaolinite clay particles was partially covered by the adsorbed polymer, which allows the bridges between the kaolinite clay particles to form. At a higher dosage of 200 ppm, the surface of the kaolinite particles was fully covered by the adsorbed polymer. In this case, the adsorbed polymer layer set a steric barrier which prevented the kaolinite particles to approach each other while not bridged. As a result, the suspension became stabilized. These settling results are consistent with those of other studies (Mpofu et al., 2003; 2004a; 2004b).

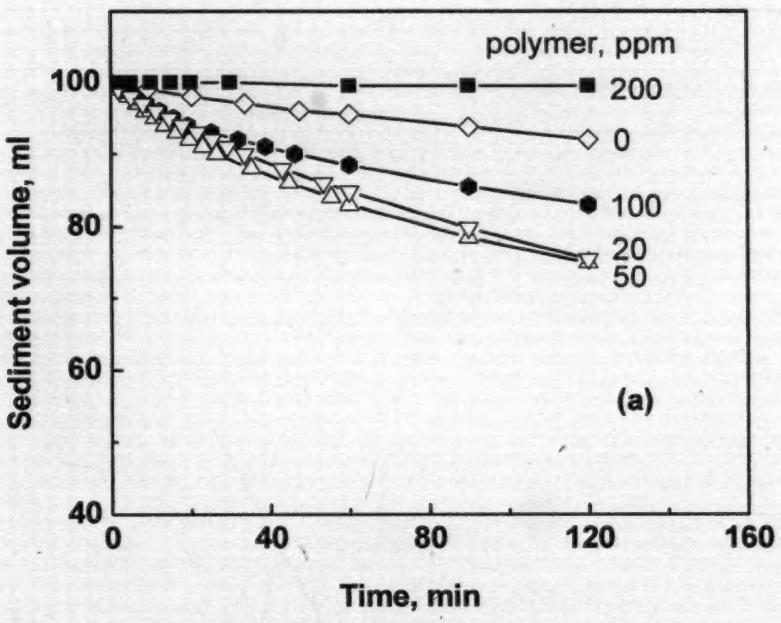

Figure 4.2a Settling curves of kaolinite clay suspensions at various polymer dosages at room temperature.

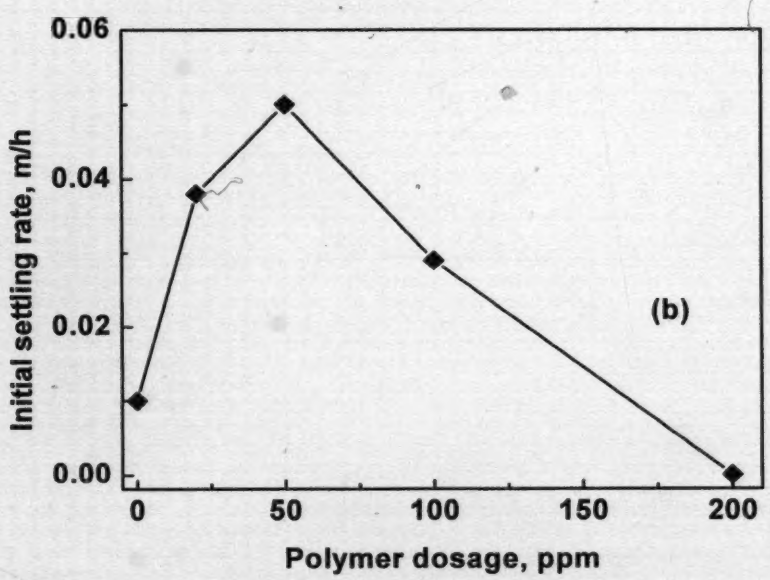

Figure 4.2b Initial settling rate as a function of polymer dosage at room temperature.

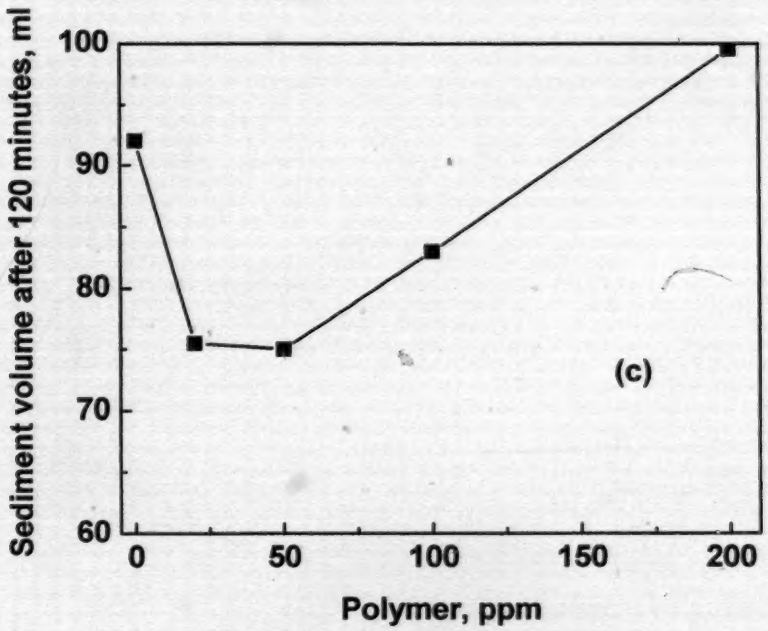

Figure 4.2c Sediment volume after 120 minutes as a function of polymer dosage at room temperature.

4.2.1.2 Results from procedure B

Figure 4.3 shows the settling results of 10 wt% kaolinite suspensions using procedure B (i.e. mixing at room temperature and then settling at 40°C). Figure 4.3a shows the settling curves at various polymer dosages. The initial settling rate increased dramatically when the polymer dosage was increased from 0 to 500 ppm (Figure 4.3b). Accordingly, the sediment volume after a settling period of 120 minutes decreased greatly from 73 to 28 ml, as shown in Figure 4.3c. Figure 4.4 shows the photograph of the settling layers of kaolinite suspensions after a settling time of 10 minutes at 40°C. A clear supernatant was obtained from the suspensions with the polymer addition.

Comparing the settling results obtained from procedure B with those from procedure A, it is clear that temperature has a great impact on the settling. Using procedure A, the maximum initial settling rate was about 0.05 m/h obtained with 50 ppm polymer addition. In contrast, an initial settling rate of 2 m/h was obtained using procedure B in the presence of 500 ppm poly(NIPAM). Using procedure A, the smallest sediment volume after a settling period of 120 minutes was about 75 ml, however it was 28 ml in the presence of 500 ppm poly(NIPAM) using procedure B. These results indicate that the sediment formed in procedure B was more compact than that in procedure A.

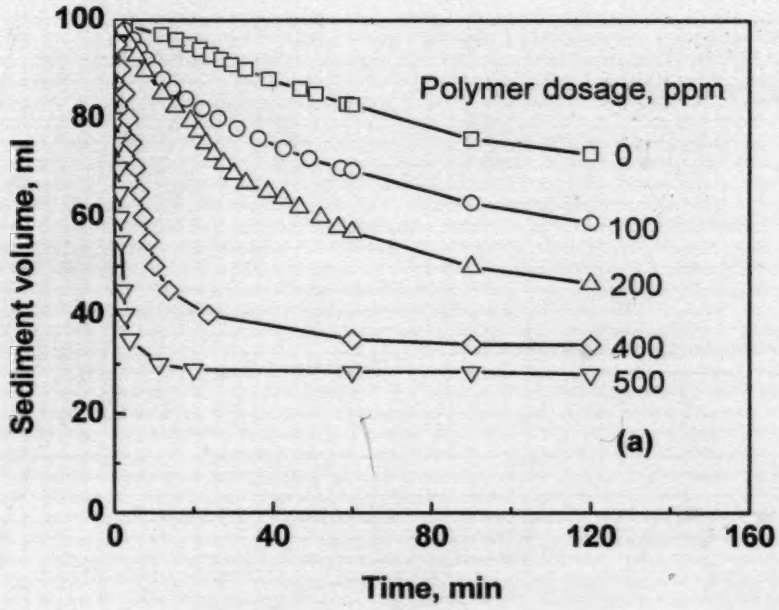

Figure 4.3a Settling curves of kaolinite suspensions at various polymer dosages at 40°C.

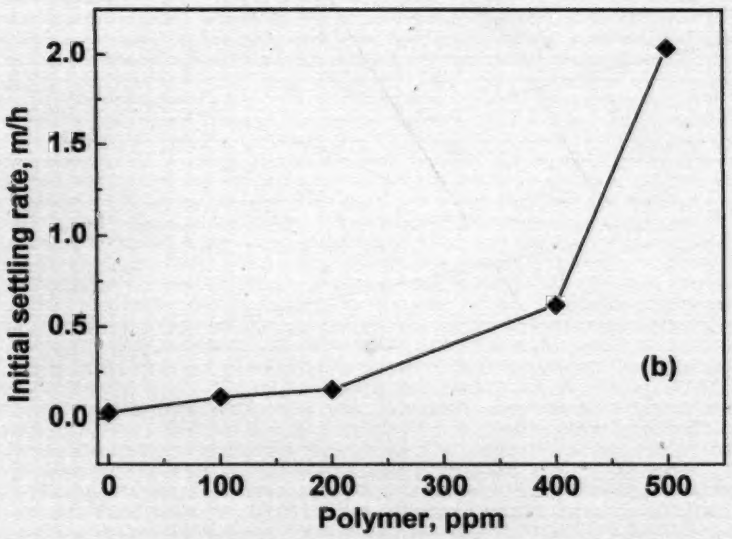

Figure 4.3b Initial settling rate as a function of polymer dosage at 40°C.

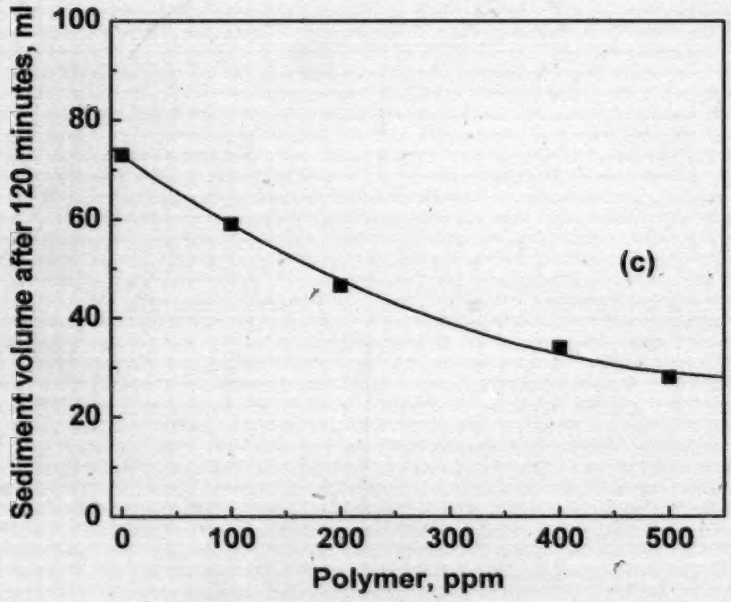

Figure 4.3c Sediment volume after a period of 120 minutes as a function of polymer dosage at 40°C.

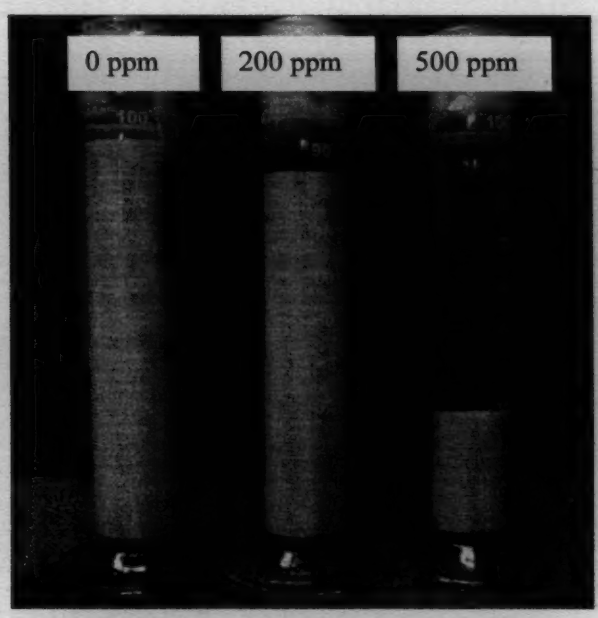

Figure 4.4 A photo showing kaolinite suspensions settling at various polymer dosages at 40°C.

4.2.2 AFM force measurements

4.2.2.1 Results obtained at room temperature

To understand the role of poly(NIPAM) as a flocculant in the settling of kaolinite suspensions, the long-range interaction and adhesion forces between kaolinite particles were measured by AFM. As a base line, Figure 4.5 shows the measured forces in a 1 mM KCl solution at pH 8.6 without polymer addition. Due to the surface irregularity of the kaolinite particles, the data are fairly scattered as anticipated. Nevertheless, it is clear that the long range interaction force was purely repulsive. To find the dominate forces contributing to the long-range repulsion, the classical DLVO theory was employed to obtain theoretical force profiles (Israelachvili, 1992). The van der Waals

force was calculated using Hamaker's microscopic approach. The reported Hamaker constant (A) of a mica/water/mica system, 2.2×10^{-20} J (Israelachvili, 1992), was used for the kaolinite /water/kaolinite system. The electrostatic double layer forces, on the other hand, were calculated numerically by solving the nonlinear Poisson-Boltzmann equation, using a constant surface potential of the kaolinite surface as a boundary condition. The kaolinite clay surface is of constant surface potential because its surface charge arises primarily from adsorbed ions from solutions (Hunter, 1993; Warszynski and Adamczyk, 1997). The measured zeta potential value (as an approximation of stern-potential, ψ_d) and calculated decay length (κ^{-1}) of the electrolytes medium were used in calculating the electric double layer forces. The zeta potential of kaolinite clay particles in a 1mM KCl solution at pH 8.6 and room temperature was measured to be about -35 mV using a Zetaphoremeter IV^{TM} (SEPHY/CAD) (Liu et al., 2002). For the 1mM KCl solution, the decay length is 9.61 nm. A program developed by Liu (2004) was used to calculate the DLVO forces. As noted in Figure 4.5, the long-range force profiles at a separate distance greater than 8 nm agree well with the theoretical profile as shown by the solid line in the figure. This indicates that the long-range forces were dominated by the electrostatic double layer interactions. The adhesion force distribution is shown in the inset of Figure 4.5. In most cases, no adhesion was detected. As the long-rang force was repulsive and the adhesion was nearly zero, the kaolinite suspension at room temperature is anticipated to be stable in 1mM KCl solutions at pH 8.6 without polymer addition. This expectation was verified in the settling tests. As discussed in the section of 4.2.1.1 above, the initial settling rate of kaolinite suspension in the absence of the polymer at room temperature was small (0.01 m/h) and the sediment volume after a

settling period of 120 minutes was 92 ml which was very close to the volume of the original suspension of 100 ml.

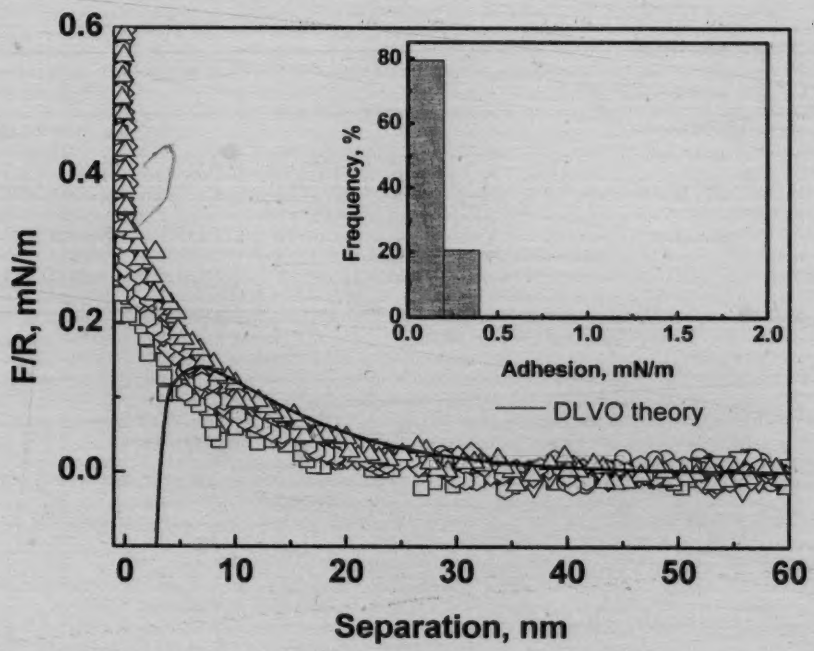

Figure 4.5 Long-range interaction and adhesion forces between kaolinite particles in 1mM KCl solutions at pH~8.6 and room temperature. The solid curve is the DLVO force profile using ψ = -35 mV, κ^{-1} = 9.61 nm and A = 2.20×10^{-20} J. The inset shows the adhesion force distribution.

Figure 4.6 shows the long-range interaction and adhesion forces between kaolinite clay particles in 1mM KCl solution and 20 ppm poly(NIPAM) at pH 8.6 and room temperature. With the polymer addition, the long-range repulsive force decreased significantly, indicating that the electrostatic double layer forces were depressed by the polymer addition. Since the polymer is non-ionic, a coverage of the surface by the

polymer would screen out the surface charge of the kaolinite particles to reduce the electrostatic repulsive forces. The flocculation of the kaolinite suspension at room temperature in the presence of poly(NIPAM) is attributed to the bridging between the kaolinite particles formed by the polymer. The bridging effect is verified by a typical retraction force profile at room temperature, as shown in Figure 4.7a. The two kaolinite surfaces, presumably connected by polymer chains, detached at a distance of 60 nm. This observation suggests that poly(NIPAM) molecules at room temperature have a long, extended structure. Due to a partial coverage of the kaolinite surface at a low polymer dosage, some free surface areas are available for polymer adsorption. The dangling tails/loops of the polymer on one surface are anticipated to contact with and adsorb onto the other surface. As a result, bridges are formed between the two surfaces. A distribution of the pull-off distances is shown in Figure 4.7b. The obtained pull-off distances are in a range of 40 to 150 nm, indicating a polydispersity of the synthesized polymer. The adhesion force distribution as shown in the inset of Figure 4.6 is centered at 0.8 mN/m. The appearance of adhesion force suggests the presence of forces holding the kaolinite particles together. The reduced repulsion and presence of adhesion would make it possible for the kaolinite particles to approach and then connect with each other, hereby resulting in flocculation between the particles. As mentioned in describing the results of settling tests using procedure A, the suspension in the presence of 50 ppm polymer exhibited an initial settling rate of 0.05 m/h and a sediment volume of 75 ml after a settling period of 120 minutes, in contrast to a negligible settling without polymer addition. This comparison indicates a practical flocculation to a large extent

due to reduced repulsion and increased adhesion between the kaolinite particles by an adequate polymer adsorption.

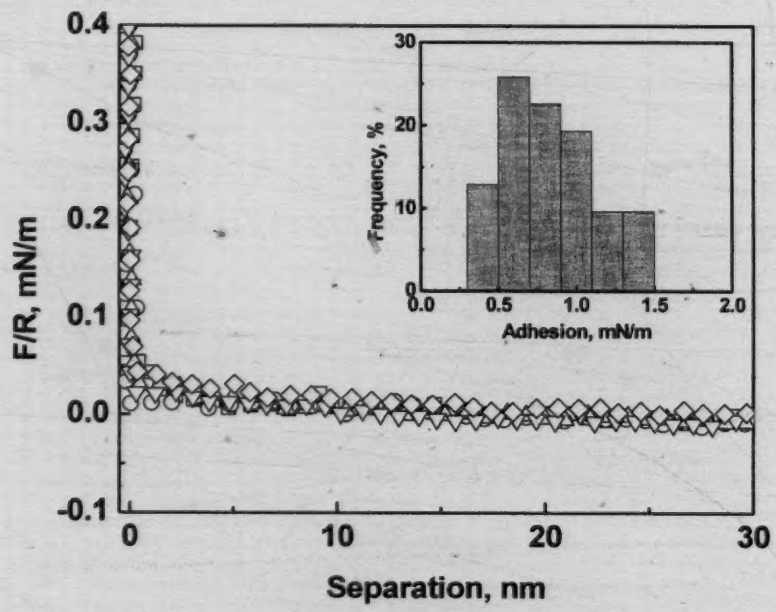

Figure 4.6 Long-range interaction and adhesion forces between kaolinite particles in a 1mM KCl solution and presence of 20 ppm poly(NIPAM) at pH~8.6 and room temperature. The inset shows the adhesion force distribution.

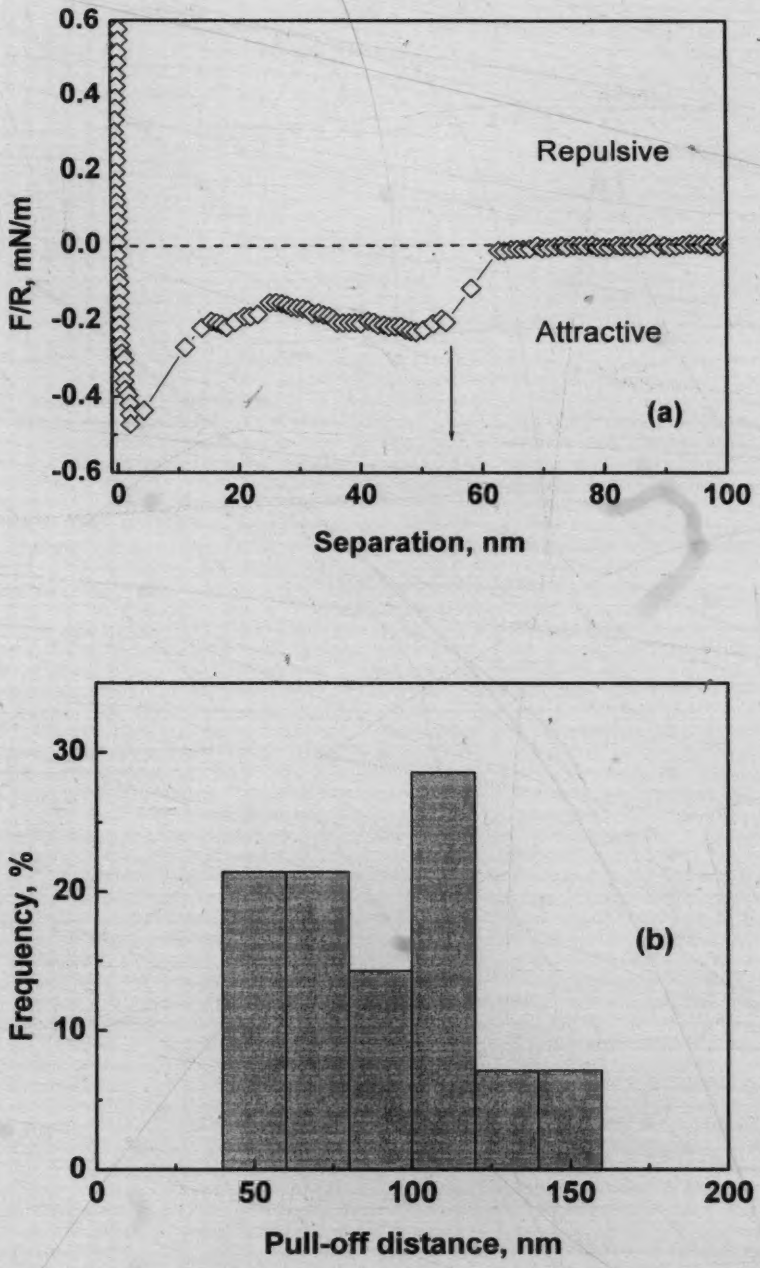

Figure 4.7 (a) A typical retraction force profile obtained between kaolinite particles in a 1mM KCl solution and presence of 20 ppm poly(NIPAM) at pH~8.6 and room temperature. (b) Distribution of the pull-off distance obtained under the same condition as (a).

Figure 4.8 shows the long-range repulsion and adhesion forces between kaolinite particles in a 1mM KCl solution containing 50 ppm polymer at pH 8.6 and room temperature. Compared with the case with 20 ppm polymer addition, the long-range repulsion became strong and the adhesion disappeared when 50 ppm polymer was present. In this case, both kaolinite surfaces were possibly fully covered by the adsorbed polymers and the adsorbed polymers set a steric barrier to prevent kaolinite particles to approach each other. The absence of adhesion indicates that the kaolinite particles hardly attached to each other. Such a condition would indicate a stable kaolinite suspension. This was verified by our settling tests where the addition of 200 ppm polymer into the suspension caused an initial settling rate to be almost zero, indicating that the suspension was very stable.

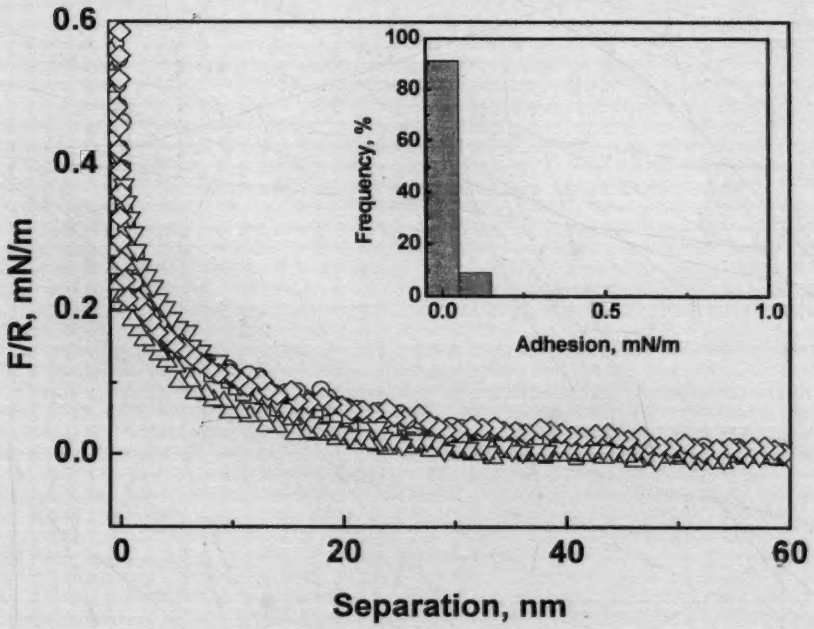

Figure 4.8 Long-range interaction and adhesion forces between kaolinite particles in a 1mM KCl solution and presence of 50 ppm poly(NIPAM) at pH~8.6 and room temperature. The inset shows the adhesion force distribution.

Figure 4.9 shows the average adhesion force (a) and the initial settling rate (b) as a function of poly(NIPAM) dosage at room temperature. Both the average adhesion force (Figure 4.9a) and initial settling rate (Figure 4.9b) as a function of poly(NIPAM) dosage exhibit similar trends. The average adhesion and the initial settling rate first increased with increasing polymer dosage to an optimal dosage, followed by a decrease with further increasing the dosage, although the maximum improvement was achieved at different dosages. This finding indicates a clear correlation between the adhesion force and the initial settling rate: the higher, the adhesion force, the higher, the initial settling rate. The difference in polymer dosages where the maximum is located is

attributed to the different surface areas of kaolinite clay particles in the two test systems. The suspension contained a large number of kaolinite particles, while there were only a few kaolinite particles in the AFM force measurement. As a result, the surface area of kaolinite particles in the suspension is much larger than that in the AFM experiments thereby depleting the polymer molecules available in solutions. It is evident that more polymer addition is required in the settling tests than in the AFM force measurement to ensure a similar availability of polymer molecules to kaolinite particles in both systems. This translates to a less amount of polymers needed in AFM force measurement to achieve the maximum adhesion force.

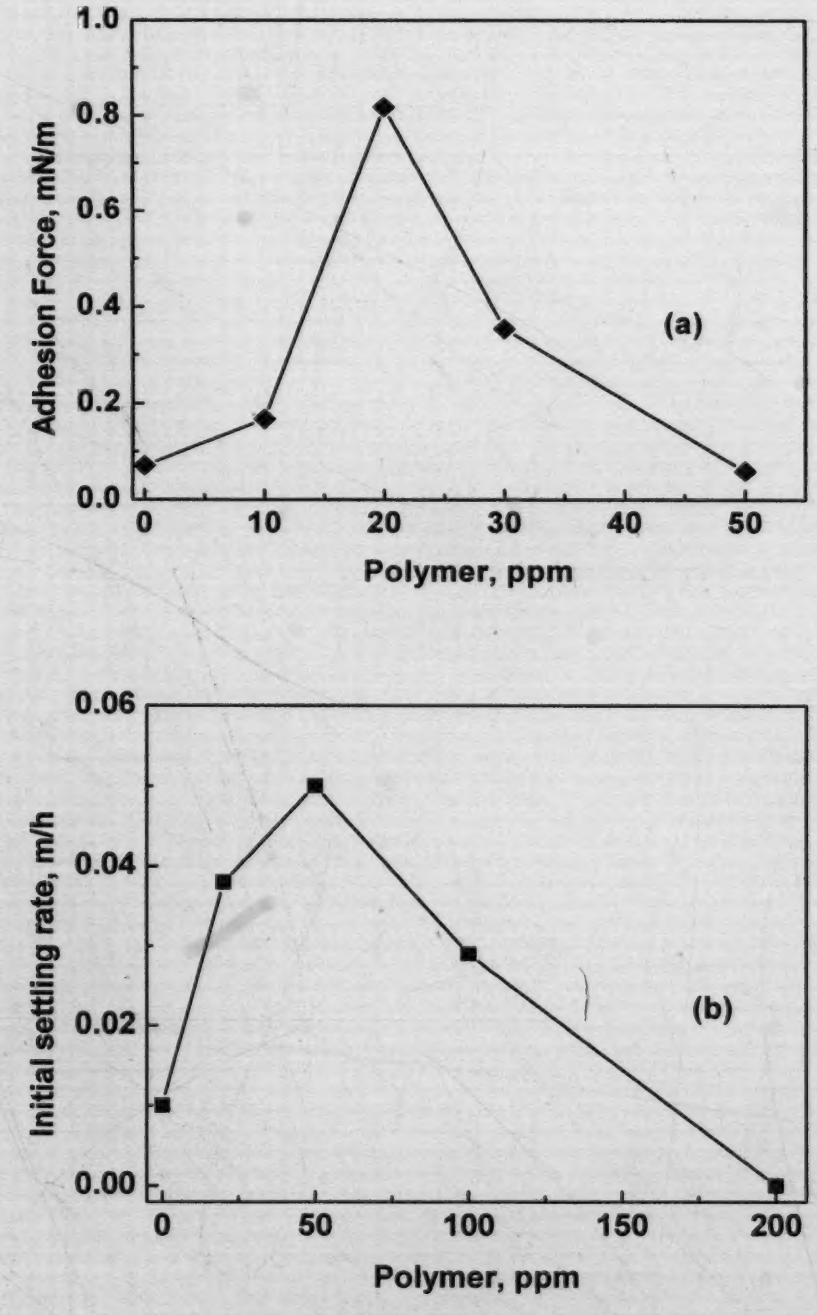

Figure 4.9 (a) Average adhesion forces as a function of polymer dosage at room temperature and pH~8.6. (b) Initial settling rate as a function of polymer dosage.

4.2.2.2 Results obtained at 40°C

As mentioned earlier, poly(NIPAM) exhibited a better flocculation behaviour using procedure B than procedure A. To understand this difference in the settling experiments, the long-range interaction and adhesion force measurements between kaolinite particles were conducted following a similar temperature-changing procedure as used in procedure B, i.e. the solution was first injected into the fluid cell at room temperature, then the solution was heated to and maintained at 40°C during the force measurement. Figure 4.10 shows the long-range interaction and adhesion forces between kaolinite particles in a 1 mM KCl solution at pH 8.6 and 40°C. Compared with the long-range repulsive forces at room temperature (Figure 4.5), the long-range repulsion at 40°C was stronger. The classical DLVO theory was used to fit the measured long-range force profiles. In the fitting procedure, the Hamaker constant (A) was the same as that used for calculating DLVO forces at room temperature (Figure 4.5). The decay length (κ^{-1}) as a function of temperature was calculated to be 12.67 nm at 40°C using the equation below (Israelachvili, 1992)

$$\kappa^{-1} = \left\{ \frac{\varepsilon \varepsilon_o k_B T}{e^2 \sum n_i(\infty) z_i^2} \right\}^{1/2} \qquad (4\text{-}3)$$

where, e is the charge on electron, n_i (∞) is the number per unit volume of the electrolyte ions of type i with valence z_i in the bulk solution far from the surface, k_B is Boltzmann's constant, T is the absolute temperature in Kelvin, ε_0 is the permittivity of vacuum, and ε is the relative permittivity of the solution. The zeta potential value of kaolinite clay particles (ψ) was set as an adjustable parameter. Figure 4.10 shows that

using a zeta potential value of -50 mV, the long-range repulsive forces were fitted well with the classical DLVO theory. It suggests that the surface potential of kaolinite particles became more negatively charged (from -35 to -50 mV) when temperature was increased from room temperature to 40°C. Ramachandram and Somasundaran (1986) also found that the surface of kaolinite particle became more negatively charged with increasing temperature. For the kaolinite surface, temperature increase would favour the formation of $Al(OH)_4^-$ and $H_3SiO_4^-$ groups, thus resulting in more negative charges on kaolinite surfaces. The adhesion force as shown in the inset of Figure 4.10 was nearly zero. Based on the long-range and adhesion forces, the kaolinite suspension is anticipated to be stable in a 1mM KCl solution at pH 8.6. As discussed earlier, without polymer addition using procedures B, the initial settling rates was 0.03 m/h, indicating a stable suspension and supporting the implications from the AFM force measurements.

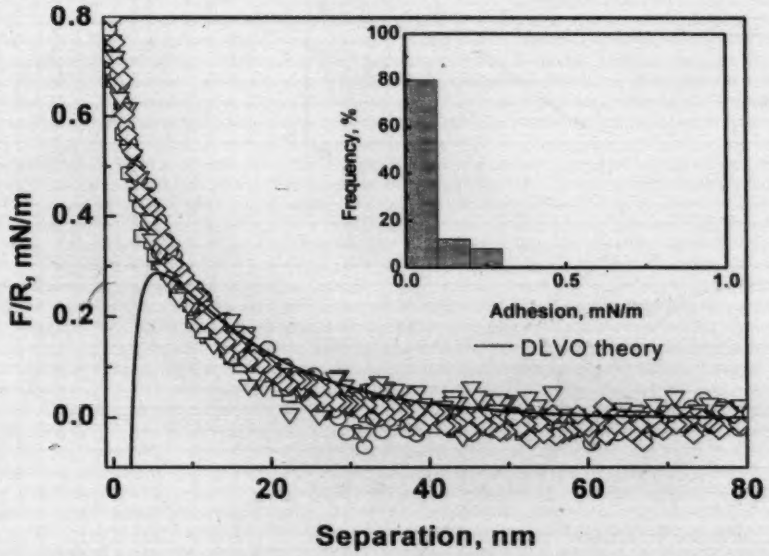

Figure 4.10 Long-range interaction and adhesion forces between kaolinite particles in a 1mM KCl solution and the absence of poly(NIPAM) at pH~8.6 and 40°C. The solid curve is the DLVO force profile using κ^{-1} = 12.67 nm, A = 2.2×10^{-20} J and a fitted potential of -50 mV. The inset shows the adhesion force distribution.

Figure 4.11 shows the long-range interaction and adhesion forces between kaolinite particles in a 1mM KCl solution containing 20 ppm polymer. Compared with the case without polymer addition (Figure 4.10), the polymer addition suppressed the long-range repulsive force and increased the adhesion force to 1.0 mN/m. Figure 4.12 shows the results with 50 ppm polymer addition at pH 8.6 and 40°C. The further polymer addition (50 ppm) suppressed the long-range repulsive force to nearly zero. The adhesion force increased drastically to 3.5 mN/m. The weak long-range repulsion and strong adhesion forces between kaolinite particles indicate that the kaolinite suspension in the presence of 50 ppm polymer will be flocculated quickly. This

expectation was verified by our settling tests using procedure B. As was shown in Figure 4.3, in the presence of 500 ppm poly(NIPAM), the initial settling rate increased to 2 m/h and the sediment volume after a settling period of 120 minutes decreased to 28 ml.

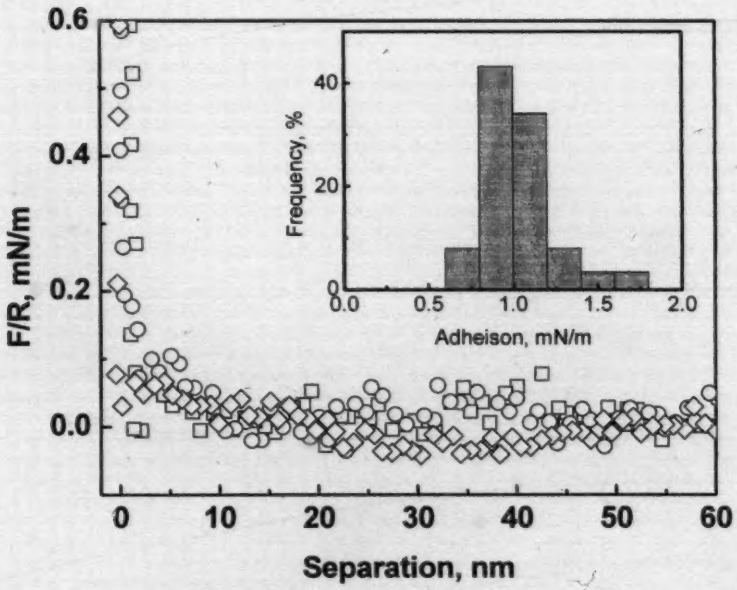

Figure 4.11 Long-range interaction and adhesion forces between kaolinite particles in 1mM KCl solution at pH~8.6 and presence of 20 ppm poly(NIPAM) at pH 8.6 and 40°C. The inset shows the adhesion force distribution.

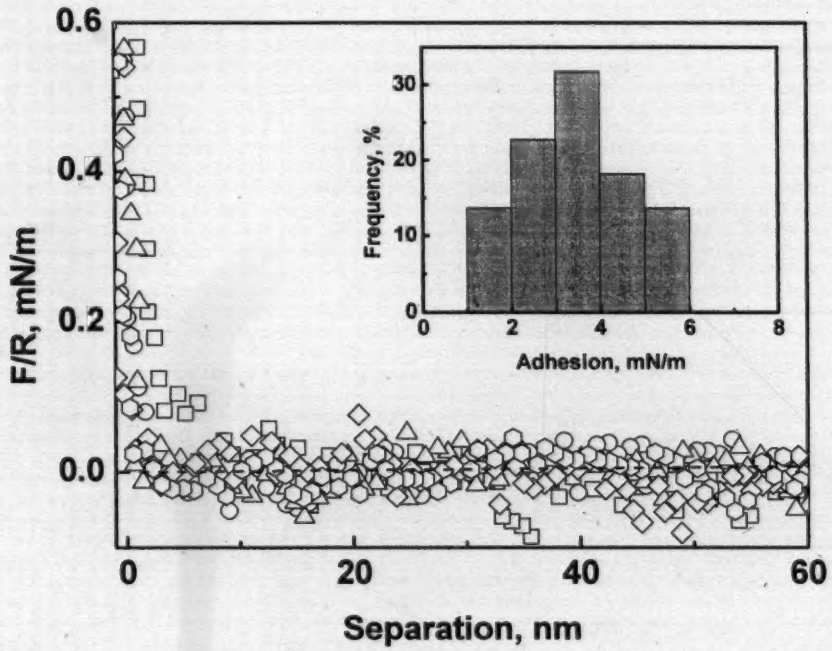

Figure 4.12 Long-range interaction and adhesion forces between kaolinite particles in 1mM KCl solution at pH~8.6 and presence of 50 ppm poly(NIPAM) at pH 8.6 and 40°C. The inset shows the adhesion force distribution.

Comparison of the AFM results obtained at room temperature with those at 40°C at the same polymer dosage of 50 ppm (Figures 4.8 and 4.12) indicates much weaker long-range repulsive forces and much stronger adhesion forces when the measurement was performed at 40°C. This observation confirms that the good flocculation of kaolinite suspension at a higher polymer dosage using procedure B is attributed to the substantially weak repulsive long-range forces and stronger adhesion forces between the kaolinite particles. The difference in the adhesion force obtained at 40°C and room

temperature can be attributed to the difference in binding strength of the polymer with clay particles and polymer confirmation.

The coil-like conformation of the polymer molecule at high temperature of 40°C was verified by the AFM results. Figure 4.13 shows a typical retraction force profile in the presence of 20 ppm poly(NIPAM) at 40°C. A detachment at a separation distance of 9 nm was observed, indicating a very compacted structure of the adsorbed polymer on the kaolinite surface. Whereas, the retraction profile obtained at room temperature (Figure 4.7a) showed a plateau of about 60 nm, i.e. a long stretch of polymer molecules, indicating an extended structure. These results and interpretation are consistent with other studies (Zareie et al., 2000; Kanazawa, 2004)

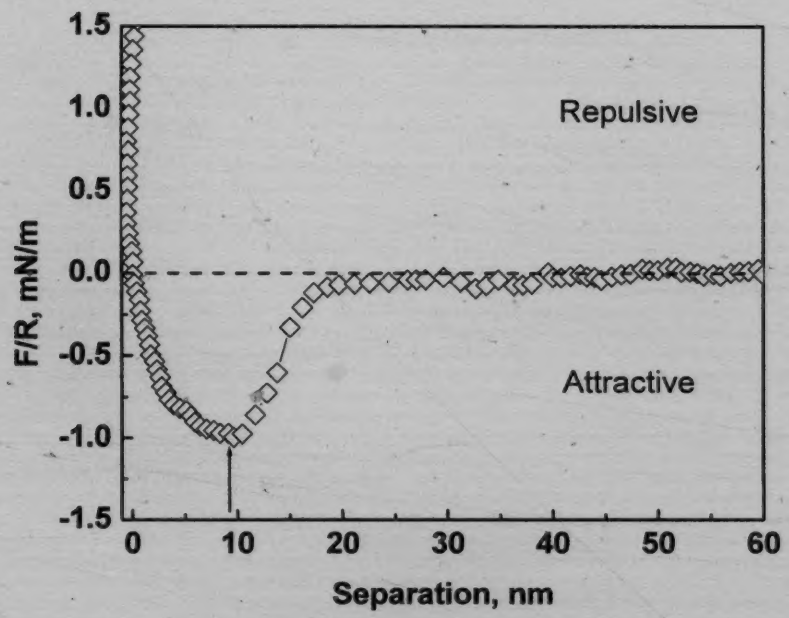

Figure 4.13 Typical retraction force profile obtained between kaolinite particles in a 1mM KCl solution and presence of 20 ppm poly(NIPAM) at pH~8.6 and 40°C.

Figure 4.14 illustrates the effect of poly(NIPAM) concentration on the interaction between two particles at room temperature and 40°C, respectively. At room temperature, the polymer molecule has a stretched structure. At a low polymer concentration (e.g. 20 ppm), the particles surface was only partially covered by the adsorbed polymers (Figure 4.14a). Some free surface areas were still available for polymer adsorption. Under such a condition, the dangling tails/loops of the polymer molecules on one surface could contact and be adsorbed onto the other surface, exhibiting bridging adhesion. At a high polymer concentration (e.g. 50 ppm), the particle surface was fully covered by the adsorbed polymers (Figure 4.14b). A steric barrier was set by the extruded tails of the adsorbed polymers thereby preventing the two particles to approach each other, leading to a strong long-range repulsion and a negligible adhesion. At 40°C, poly(NIPAM) molecule became coiled. At a low polymer concentration (e.g. 20 ppm), the adsorbed polymers caused a partial coverage of the particle surface (Figure 4.14c). Bridging was formed between the two particles by the adsorbed polymers with a coil-like structure. At a high polymer concentration (e.g. 50 ppm), the surface coverage of the particles by the adsorbed polymers increases. As the polymer molecule was coiled, the surface of the particles was still partially covered (Figure 4.14d). The number of the polymer bridges was significantly increased, resulting in a strong adhesion force (e.g. 3.5 mN/m at a polymer concentration of 50 ppm).

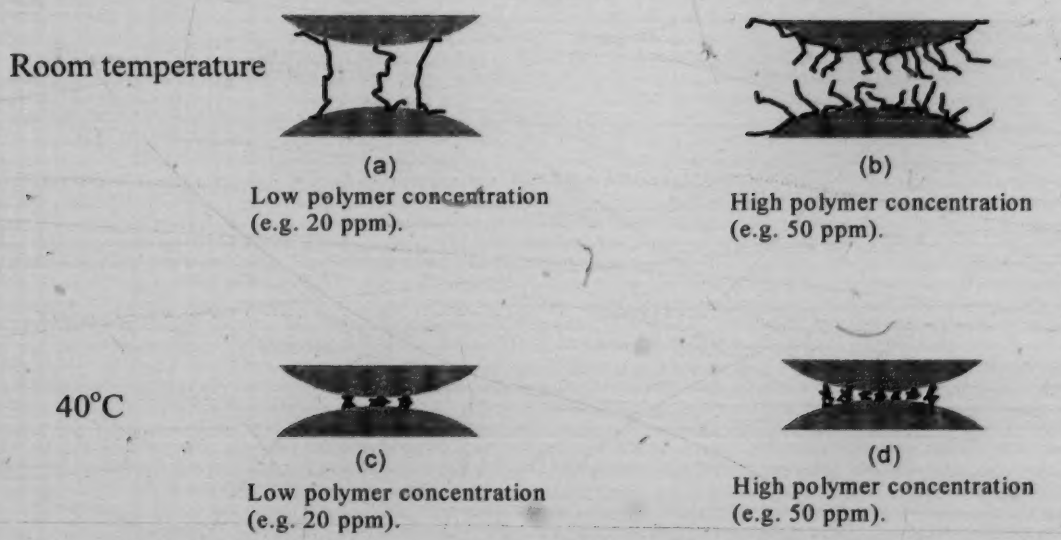

Figure 4.14 Role of polymer concentration in fine kaolinite flocculation (Schematic). At room temperature: (a) Low polymer concentration (e.g. 20 ppm). The surface of the particles was partially covered by the adsorbed polymer molecules with a stretched structure. Bridging was formed between the two particles by the adsorbed polymers. (b) High polymer concentration (e.g. 50 ppm). The surface of the particles was fully covered by the adsorbed polymer molecules. A steric repulsion was caused by the extruded polymer tails. At 40°C: (c) Low polymer concentration (e.g. 20 ppm). Bridgings were formed between two particles by the adsorbed polymers with a coil-like structure. (d) High polymer concentration (e.g. 50 ppm). The surface coverage of the particles by the adsorbed polymers was increased. More polymer bridges were formed between the two particles by the adsorbed polymer molecules.

The conformation change of poly(NIPAM) molecule is related to its chemical structure. As shown in Figure 2.3, there is a hydrophilic group (-CONH-) and a hydrophobic group ($-CH(CH_3)_2$) on the polymer side chain. Ramon et al. (2001) and Katsumoto et al. (2004) found that in an aqueous solution, there are relatively strong

hydrogen bonds between the hydrophilic group (-CONH-) and water molecules at room temperature. Thus, the polymer is highly soluble and exhibits an extendable structure. When temperature is increased, hydrogen bonds between the hydrophilic groups and water molecules are broken and intra-molecular hydrogen bonds, C=O····H-N, become predominant. As a result of such intra-molecular interactions, the polymer molecules become coiled.

Figure 4.15 shows a schematic diagram of the flocculation mechanism using poly(NIPAM) under procedure B. The polymer molecules with a stretched structure were first mixed with clay suspension at room temperature. Under such condition, particles could adsorb onto different sites of the long extended polymer chains. When temperature was increased to 40°C, the polymer chains became coiled. The adsorbed particles were then brought together, leading to compacted flocs.

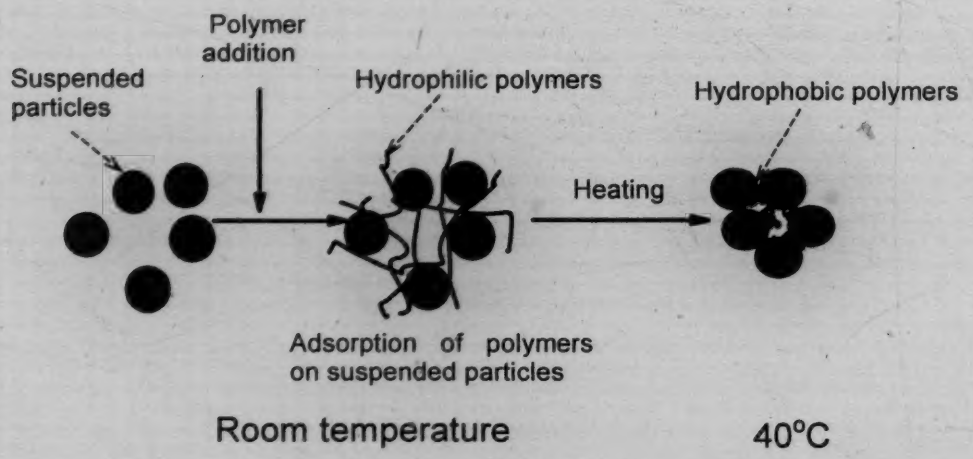

Figure 4.15 Schematic diagram of the flocculation mechanism using a temperature-sensitive polymer (poly(NIPAM) for procedure B.

Figure 4.16 shows the average adhesion force and the initial settling rate as a function of polymer dosage at 40°C. The trends of the average adhesion forces (Figure 4.16a) and the initial settling rate in response to the change of poly(NIPAM) dosage (Figure 4.16b) are similar, i.e. they both increased with increasing polymer dosage.

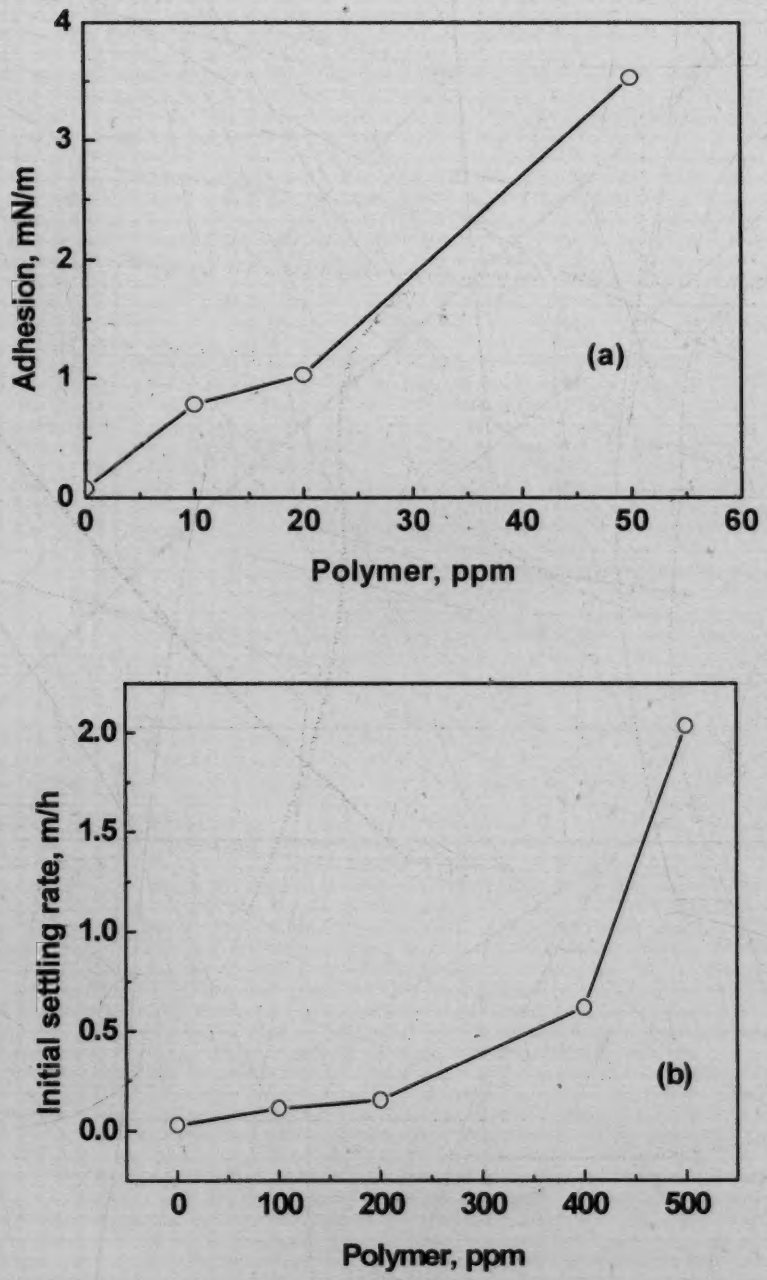

Figure 4.16 (a) Average adhesion forces as a function of polymer dosage at 40°C. (b) Initial settling rate as a function of the polymer dosage using settling procedure B.

4.3 Summary

(1) In the presence of poly(NIPAM), suspension temperature shows an important impact on the settling rate of kaolinite clays. Poly(NIPAM) exhibits a better flocculation performance with a wider operational dosage range using procedure B than using procedure A.

(2) Results of AFM force measurement were consistent with the settling results. A weaker long-range repulsive force and a stronger adhesion force were obtained at 40°C than that at room temperature.

(3) Poly(NIPAM) molecules exhibit a long, extended structure at room temperature, and a coil-like conformation at 40°C. It is this conformational change of the polymer molecules that results in a better settling using procedure B than procedure A.

Chapter 5 Kaolinite clays in Aurora process water

As the majority of water used in oil sands processing is from recycle process water, it is of great practical significance to study the flocculation behaviour of the polymer in a plant recycle process water. Because chemicals are widely used in bitumen extraction process, a high level of salts and organics is anticipated in the process water. A typical ions analysis of Aurora process water was given by Zhao et al. (2006), as listed in Table 5-1.

Although the polymer exhibits a good flocculation performance for kaolinite clay suspensions prepared in de-ionized water, its flocculation behaviour in suspensions prepared in process water remains to be investigated. In this part, the flocculation behaviour of the polymer in Aurora process water is discussed.

Table 5-1 Inorganic components of Aurora process water

	K^+	Na^+	Mg^{2+}	Ca^{2+}	Cl^-	NO_3^-	SO_4^{2-}	HCO_3^-
mM	0.37	22	0.79	1.2	12	0.03	0.66	11

5.1 Settling results

5.1.1 Results from procedure A

Figure 5.1a shows the settling curves of 10 wt% kaolinite suspensions prepared in Aurora process water using procedure A. A similar trend of the settling results was

obtained as those in de-ionized water, i.e. the initial settling rate first increased from 0.03 to 0.4 m/h when the polymer dosage was increased from 0 to 80 ppm, and then decreased with further increasing the polymer dosage (Figure 5.1b). The sediment volume after a settling period of 120 minutes first decreased from 71 to 40 ml (Figure 5.1c). After this dosage (i.e. 80 ppm), it increased with increasing polymer addition.

Compared with the settling results obtained from the suspensions prepared in de-ionized water (Figure 4.2), the initial settling rates were slightly higher and the sediment volumes were smaller for the suspensions prepared in Aurora process water. For example, the maximum initial settling rate reached 0.4 m/h but it was only 0.05 m/h for the suspension prepared in de-ionized water. The smallest sediment volume after a settling period of 120 minutes was 40 ml compared to 75 ml for the suspension prepared in de-ionized water. The settling improvements can be attributed to the synergic effect of the polymer and divalent cations contained in process water on the flocculation of the suspensions (Sworska et al., 2000; Long et al. 2006).

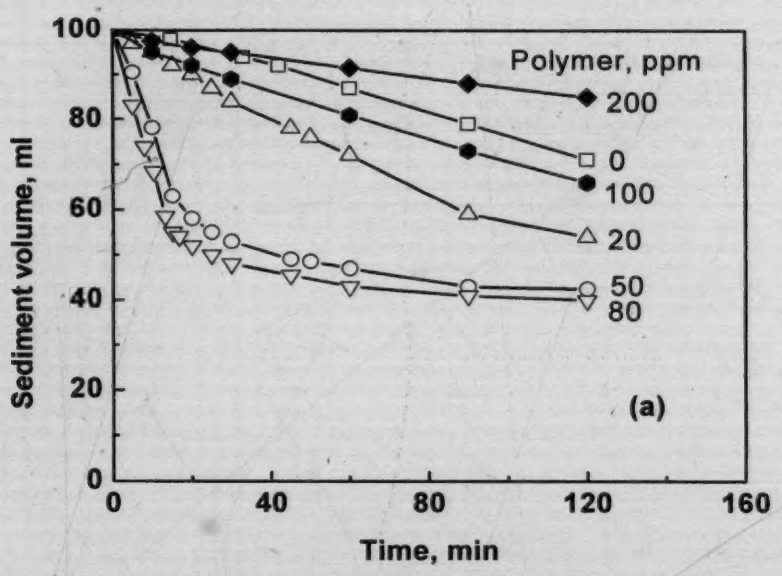

Figure 5.1a Settling curves of kaolinite clay suspensions at various polymer dosages at room temperature (procedure A).

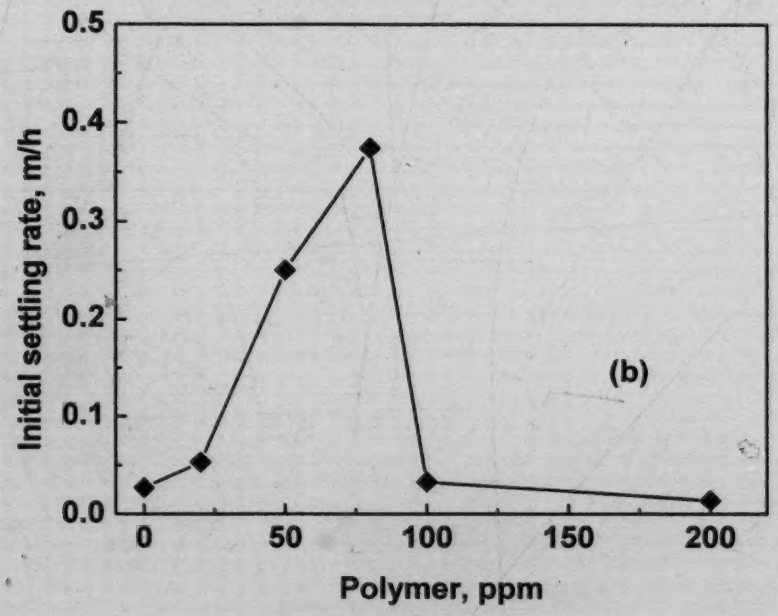

Figure 5.1b Initial settling rate as a function of polymer dosage at room temperature.

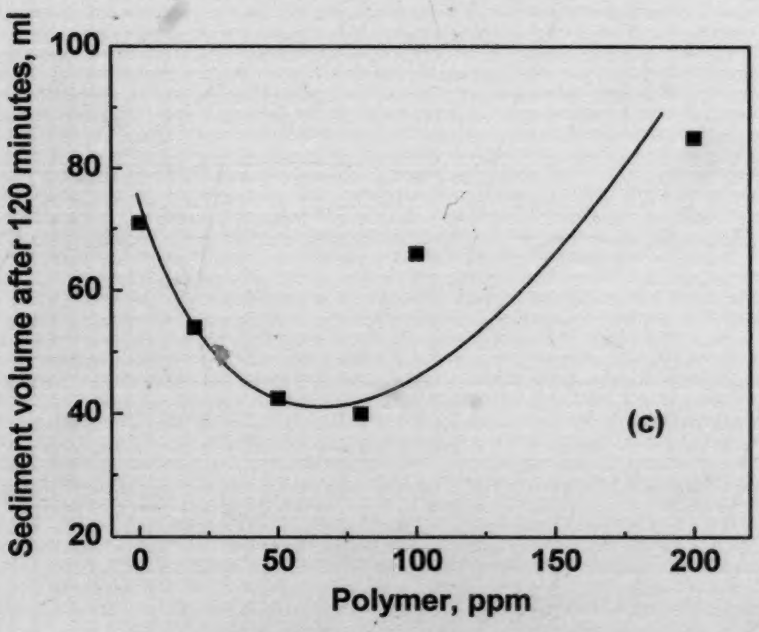

Figure 5.1c Sediment volume after a settling period of 120 minutes as a function of polymer dosage at room temperature.

5.1.2 Results from procedure B

Figure 5.2 shows the settling results of 10% clay suspensions prepared in Aurora process water following procedure B. The settling curves were shown in Figure 5.2a. When the polymer dosage increased from 0 to 500 ppm, the initial settling rate continuously increased from 0.05 to 2.9 m/h (Figure 5.2b) and the sediment volume decreased from 51 to 23 ml (Figure 5.2c). In contrast, for the case of procedure A (i.e. without a temperature change), there was an optimal polymer dosage at about 80 ppm (Figure 5.1), where the initial settling rate was maximum and the sediment volume was

smallest. This indicates that the polymer exhibits a different flocculation behaviour using procedure B from that using procedure A.

Compared with those settling results obtained from the suspensions prepared in de-ionized water at 40°C (Figure 4.3), a slightly higher initial settling rate and smaller sediment volume were obtained from the suspensions prepared in Aurora process water (Figure 5.2). For example, the initial settling rate was 2 m/h for the suspension prepared in de-ionized water with 500 ppm polymer addition (Figure 4.3b) while it reached 2.9 m/h for the suspension prepared in Aurora process water under the same condition (Figure 5.2b). This settling improvement may be due to the synergetic effect between the polymer and the cations contained in Aurora process water.

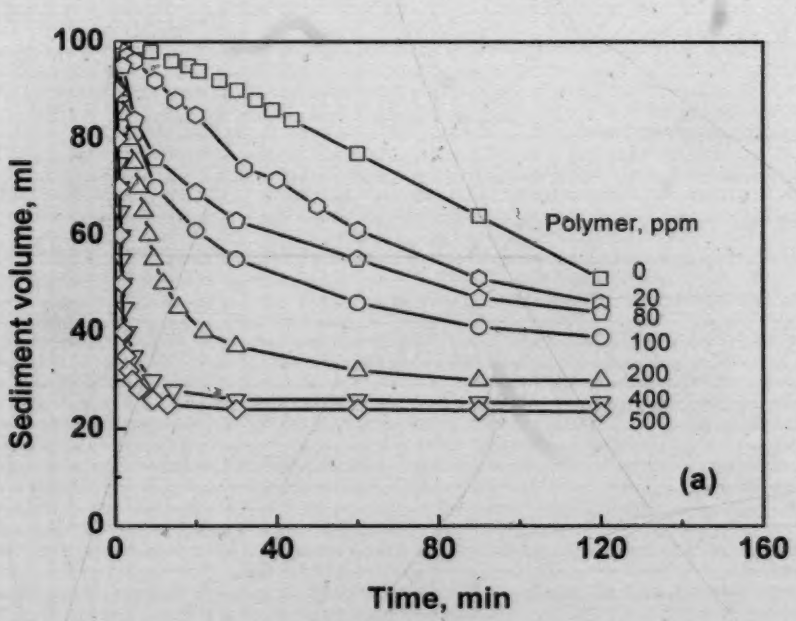

Figure 5.2a Settling curves of kaolinite clay suspensions at various polymer dosages at 40°C (procedure B).

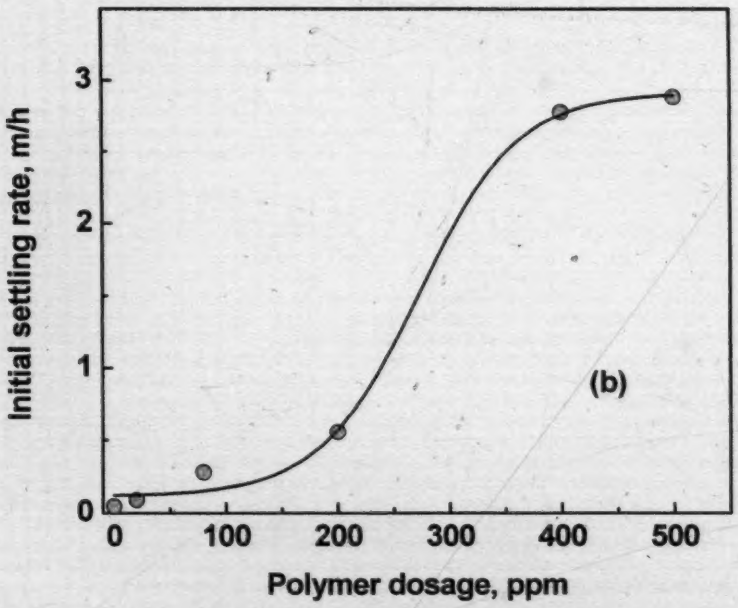

Figure 5.2b Initial settling rate as a function of polymer dosage at 40°C.

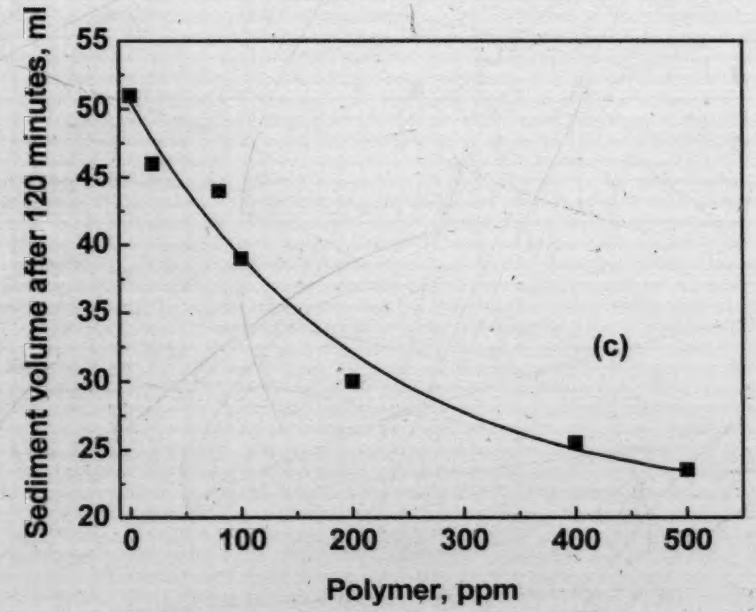

Figure 5.2c Sediment volume after a settling period of 120 minutes as a function of polymer dosage at 40°C.

5.2 AFM force measurement

5.2.1 Results obtained at room temperature

As plant recycle process water is a complex system, to understand the flocculation behaviour of the polymer in the process water, direct surface force measurement between two kaolinite particles was conducted in the supernatants of the suspensions after the setting experiments. Figure 5.3 shows the long-range interaction and adhesion forces between two kaolinite particles in the supernatant of the suspension in the absence of the polymer addition at room temperature. The long-range interaction was repulsive and the adhesion forces were negligible. The measured long-range repulsive forces were compared with the classical DLVO theoretical values. In the calculation of the DLVO theoretical forces, the Hamaker constant (A) was 2.2×10^{-20} J. The decay length (κ^{-1}) was calculated to be 1.52 nm based on ionic strength of Aurora process water. The zeta potential value (ψ) of kaolinite particles in Aurora process water at room temperature was measured to be about -27 mV. As shown in Figure 5.3, the long-range force profile agrees well with the DLVO theoretical profile at a separate distance greater than 5 nm. The measured long-range repulsive force and negligible adhesion forces indicate that the suspension would be stable under such conditions, which was verified by the settling tests in the section of 5.1.1.

Compared with those obtained in a 1mM KCl solution (Figure 4.5), the long-range forces between kaolinite particles in Aurora process water were less repulsive, indicating the electrostatic double layer was depressed. Because a large amount of cations was contained in Aurora process water, especially the presence of calcium and

magnesium, the adsorption of cations on the surface of kaolinite particles decreased its negative charge density. Thereby the double layer forces were depressed which made it easier for kaolinite particles to approach to each other.

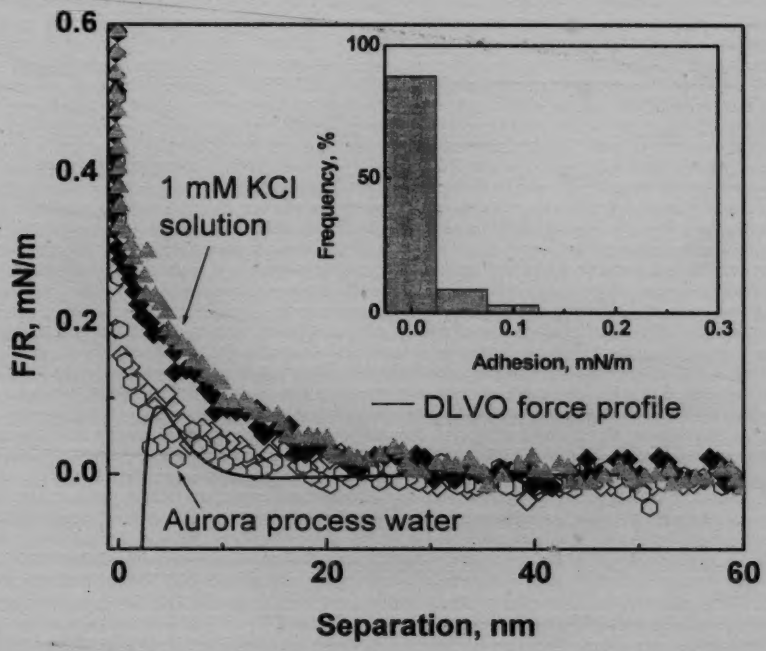

Figure 5.3 Long-range interaction and adhesion forces between kaolinite-kaolinite particles in the supernatant of the suspension in the absence of poly(NIPAM) at room temperature. The solid curve was obtained with the DLVO theory using ψ= -27 mV, κ^{-1} = 1.52 nm and A = 2.20×10^{-20} J. The inset shows the adhesion forces distribution.

Figure 5.4 shows the long-range interaction and adhesion forces between two kaolinite particles in the supernatant of kaolinite suspension with 80 ppm polymer addition at room temperature. The long-range forces between the two kaolinite particles became less repulsive. The adhesion was centered at 0.9 mN/m. Both the depressed

repulsion and the presence of adhesion forces contribute to the flocculation between kaolinite particles. A bridging effect of the polymer was found to cause the flocculation of kaolinite suspension at room temperature. The bridging effect was verified by the retraction profiles obtained in our AFM force measurements. Figure 5.5 shows a typical retraction profile between two kaolinite particles in the supernatant of the suspension in the presence of 80 ppm polymer at room temperature. The profile with a plateau detached at a long distance of 120 nm, indicating a bridge between the two surfaces.

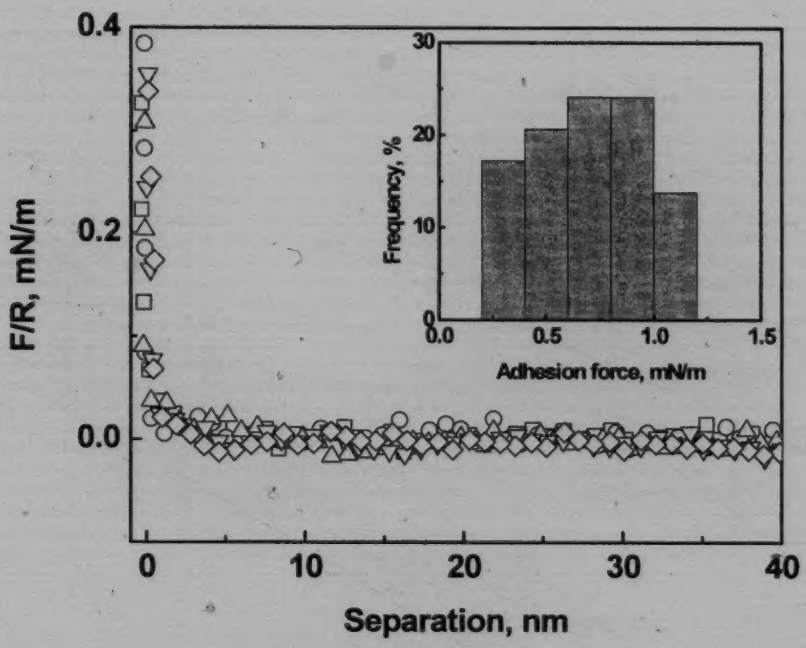

Figure 5.4 Long-range interaction and adhesion forces between two kaolinite particles in the supernatant of the suspension in the presence of 80 ppm polymer at room temperature. The inset shows the normalized adhesion force distribution.

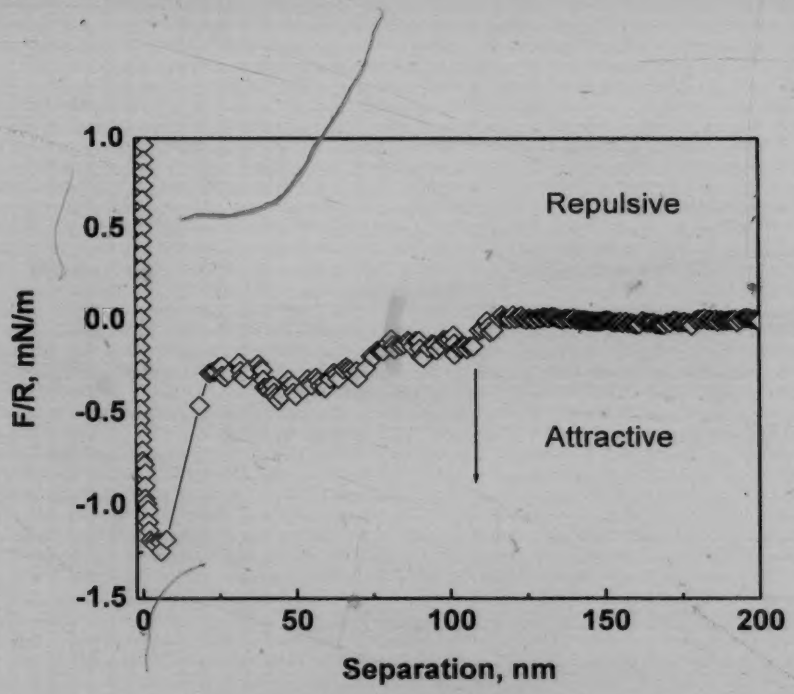

Figure 5.5 Typical retraction force profile recorded between two kaolinite particles in the supernatant of the suspension in the presence of 80 ppm polymer at room temperature.

With a further increase in the polymer dosage, the surfaces of kaolinite particles would be fully covered by the polymer. The adsorbed polymer layer set a steric barrier to prevent kaolinite particles to approach. This expectation was verified by results in Figure 5.6 which shows the long-range interaction and adhesion forces between two kaolinite particles in the supernatant of the suspension with 100 ppm polymer addition at room temperature. The long-range repulsion forces became strong and the adhesion forces became nearly zero, indicating a stable suspension at such conditions.

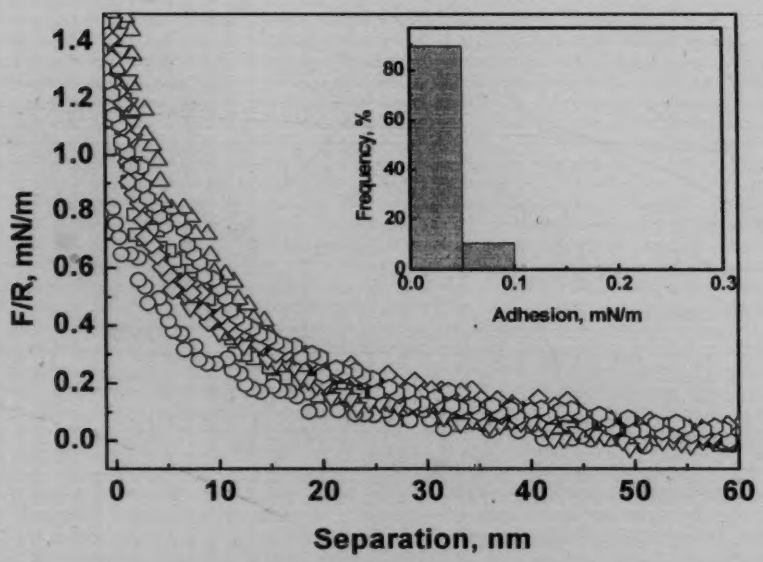

Figure 5.6 Long-range interaction and adhesion forces between two kaolinite particles in the supernatant of the suspension and presence of 100 ppm polymer at room temperature. The inset shows the normalized adhesion force distribution.

5.2.2 Results obtained at 40°C

As discussed in the settling tests, the suspension temperature plays an important role in the flocculation performance of the polymer in the suspensions prepared in Aurora process water. To understand the flocculation behaviour of the polymer in process water with a temperature change, the long-range interaction and adhesion forces between two kaolinite particles were measured following a similar temperature-changing procedure as used in procedure B. The supernatants of kaolinite suspensions were first slowly injected into the fluid cell at room temperature. Then the solution was heated to and maintained at 40°C. The force measurements were conducted at this temperature. Figure 5.7 shows the long-range interaction and adhesion forces between

two kaolinite particles in the supernatant of the suspension without polymer addition at 40°C. The long-range forces were repulsive and the adhesion forces were negligible. The classical DLVO theory was used to fit the measured long-range forces. The fitting procedure was the same as that used in de-ionized water. The decay length (κ^{-1}) was calculated to be 2 nm from the equation of 4-3. The Hamaker constant (A) is the same as that used at room temperature.The zeta potential value of kaolinite particle (ψ) was set as an adjustable parameter. As shown in Figure 5.7, when the zeta potential value was set as -33 mV, the measured long-range force profiles were well fitted with the DLVO theory. It suggests that the zeta potential of kaolinite particle became more negative (from -27 to -33 mV) when the temperature was increased from room temperature to 40°C. The strong long-range repulsion and negligible adhesion indicate that the suspension would be stable at such conditions.

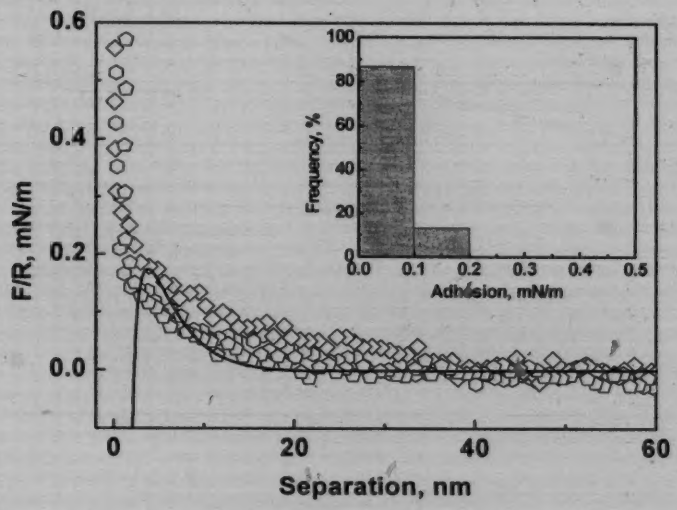

Figure 5.7 Long-range interaction and adhesion forces in the supernatant of the suspension in the absence of polymer at 40°C. The solid curve was obtained with the DLVO theory by using κ^{-1}= 2.0 nm and A= 2.20×10^{-20} J and a fitted potential of -33 mV. The inset shows the normalized adhesion force distribution.

Figure 5.8 shows the long-range interaction and adhesion forces between two kaolinite particles in the supernatant of a suspension in the presence of 500 ppm polymer at 40°C. The long-range repulsive forces became nearly zero and the adhesion became strong (centered at 3.0 mN/m). The negligible repulsion and strong adhesion would indicate that kaolinite particles could approach to each other and hold together to form dense flocs. These findings were verified by our settling tests in section 5.1.2.

The dense flocs were related to the conformation change of the polymer molecules when temperature increased from room temperature to 40°C. The conformation change was verified by our AFM force profiles. Figure 5.9 shows a typical retraction profile in the supernatant of the suspension in the presence of 200 ppm polymers at 40°C. It detached at a small separation distance of 4 nm, indicating a compact structure of the adsorbed polymer between the two kaolinite particles. However, at room temperature the retraction profile was detached at a much larger distance of about 120 nm (Figure 5.5), indicating an extended structure of the adsorbed polymer.

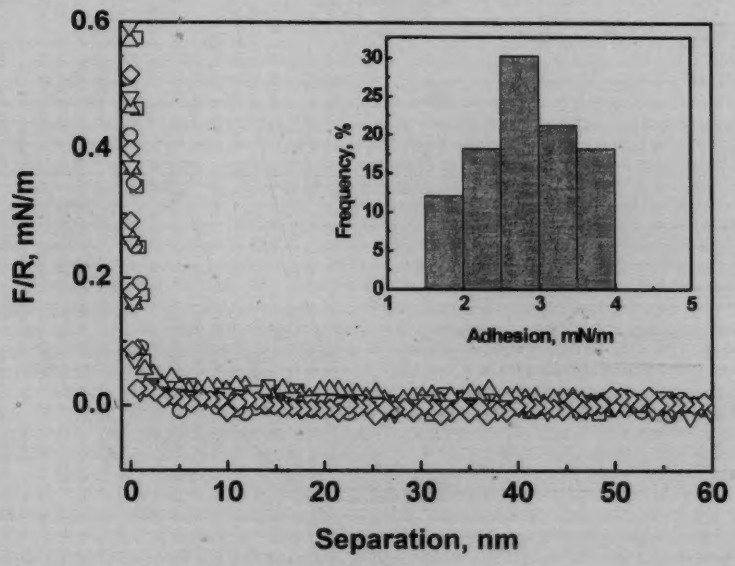

Figure 5.8 Long-range interaction and adhesion forces in the supernatant of the suspension in the presence of 500 ppm polymer. The inset shows the adhesion force distribution.

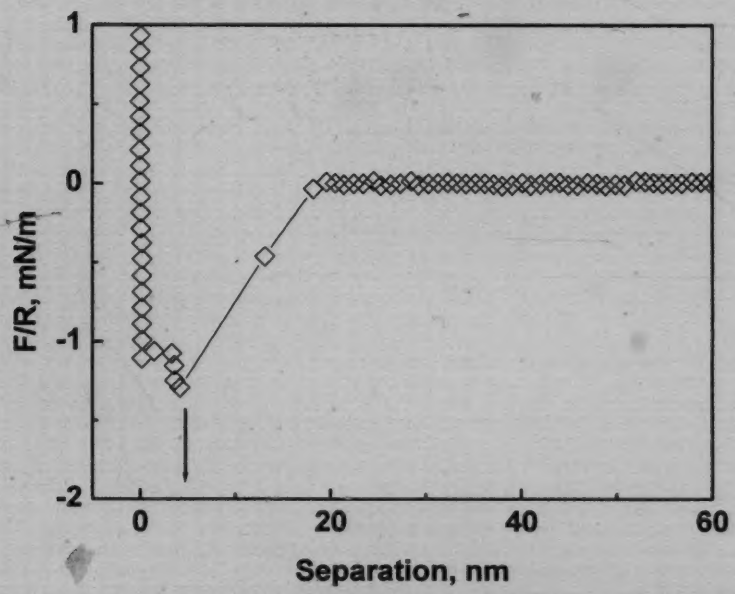

Figure 5.9 Typical retraction force profile recorded between two kaolinite particles in the supernatant of the suspension in the presence of 200 ppm polymer at 40°C.

5.2.3 Relationship of the settling results and measured adhesion forces

The stability of a clay suspension is controlled by the colloidal forces between clay particles. As discussed above, small repulsive forces can make the particles to easily approach to each other and strong adhesion forces can hold them together to form large and dense flocs. Figure 5.10 shows the initial settling rates as a function of adhesion forces between two kaolinite particles. A linear relationship was observed, indicating that adhesion strength is good measurement of flocculation and hence initial settling rate.

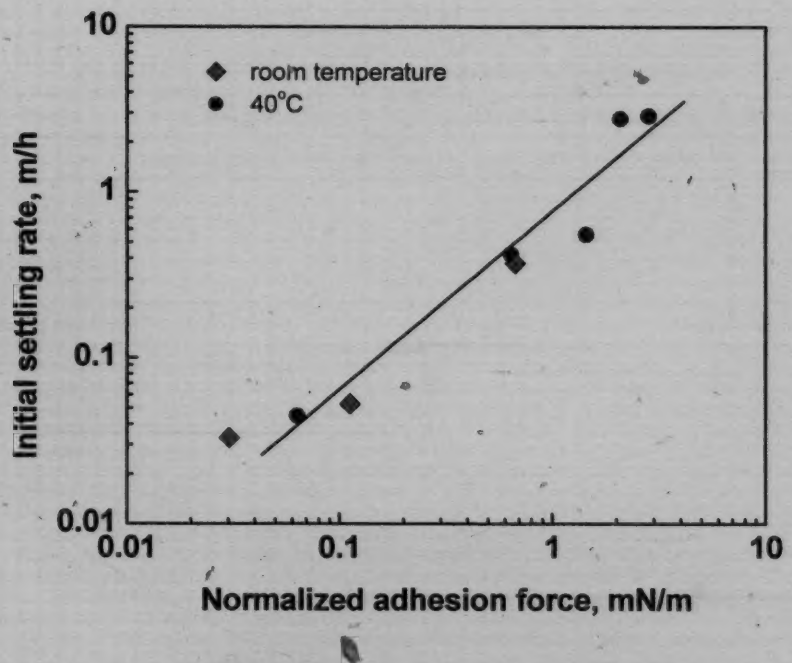

Figure 5.10 Initial settling rates as a function of adhesion forces between two kaolinite particles.

5.3 Summary

(1) The prepared temperature-sensitive polymer was tested in the flocculation of kaolinite suspensions in Aurora process water.

(2) The polymer exhibited a similar behavior in Aurora process water as that in de-ionized water. A little higher initial settling rate and smaller sediment volume were observed for suspensions prepared in Aurora process water than those prepared in de-ionized water due to the synergetic effect between the polymer and divalent cations contained in Aurora process water.

(3) There is a clear linear relationship between flocculation performance measured by initial settling rate and adhesion forces: the higher, the initial settling rate; the higher, the adhesion force.

(4) Coiled structure of a polymer flocculant shows a better flocculation performance.

Chapter 6 Oil Sands System

It is known that poor processability of low-grade oil sands ores is mainly attributed to their high fines content. As the tested polymer could effectively flocculate clay fines, it was studied as a process aid to treat low-grade oil sands ores. Due to the polymer temperature sensitivity, two extraction procedures (I and II) similar to the settling procedures were designed. In procedure I, both oil sands slurry conditioning and bitumen flotation were carried out at room temperature. In procedure II, oil sands slurry was first conditioned at room temperature and then bitumen flotation was conducted at 40°C.

6.1 Results from procedure I

Figure 6.1 shows bitumen recovery as a function of the polymer dosage using extraction procedure I at room temperature. Here, the polymer dosage is referred to the polymers initially added in bitumen extraction in term of the total slurry volume. Bitumen recovery decreased with the polymer addition. For example, in the absence of the polymer, the bitumen recovery after one hour flotation was about 25% but it reduced to 15% with 40 ppm polymers addition. Figure 6.2 shows the froth quality as a function of the polymer dosage at room temperature. The froth quality is given by bitumen to solids (B/S) and bitumen to water (B/W) mass ratio in the collected froth. The value of B/S and B/W decreased drastically with the polymer addition, indicating an increase of solids and water content in the bitumen froth.

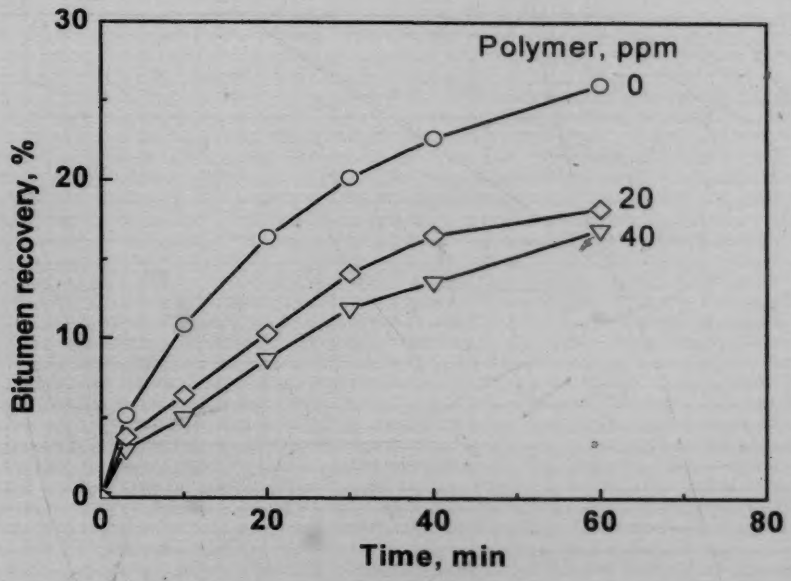

Figure 6.1 Bitumen recovery at various polymer dosages using extraction procedure I at room temperature.

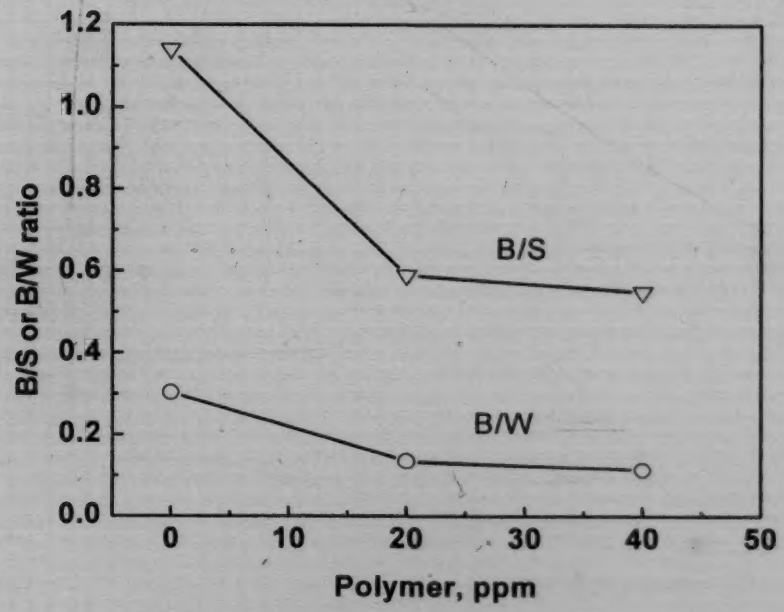

Figure 6.2 Bitumen froth quality (B/S and B/W) at various polymer dosages at room temperature.

Figure 6.3 shows the settling curves of oil sands tailings slurry. The tailings samples taken after the extraction experiments were directly used to conduct the settling tests at room temperature. The added polymers in in the extraction process did not exert significant influence on the flocculation of the tailings slurry at room temperature.

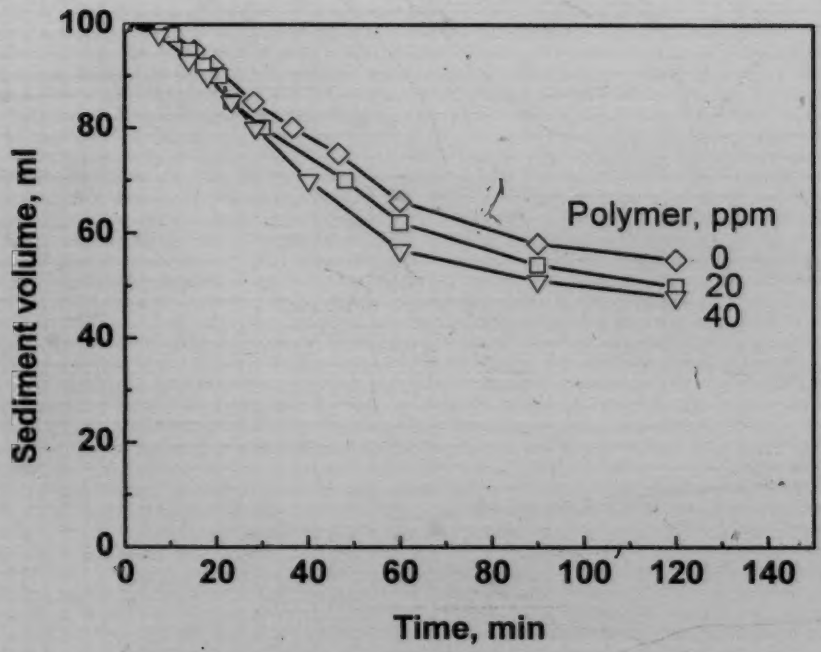

Figure 6.3 Settling curves of oil sands tailings at various polymer dosages at room temperature.

It is known that several factors, including interactions between fines and bitumen, the attachment of air bubbles to bitumen surface, and interactions between fines and air bubbles, play crucial roles in oil sands processing. At room temperature, the polymer has a conformation of a long, extended chain with two different groups: hydrophilic

groups (acrylamide) and hydrophobic groups (isopropyl) (Figure 2.3). The hydrophilic groups would allow the polymer to possibly adsorb on the surface of fines by hydrogen bonding (Peng and Di, 1994; Long et al., 2006) while the hydrophobic groups make it possible to adsorb to the surface of air bubbles or bitumen droplets. Due to the diversity of the polymer molecular weights (Figure 4.7b), both small and large flocs are possible to form. Particles often form small flocs when low molecular weight polymers were used while larger flocs are formed for high molecular weight polymers. As the polymer has a long, extended conformation at room temperature (Figures 4.7a and 5.5), the formed flocs are anticipated to have a loose structure. Since the polymer contains hydrophobic groups: isopropyl (Figure 2.3), the polymer can adsorb on the surface of air bubbles or bitumen droplets. As a result, the attachment efficiency between air bubbles and bitumen droplets could be reduced, resulting in both a decreased bitumen recovery and poor froth quality at room temperature (Figures 6.1 and 6.2). If the formed flocs were large, they could enter into the bitumen froth or settled to the tailings slurry, depends on the gravity and buoyancy of the oil sands slurry. As the floc structure at room temperature is loose, air bubbles can be potentially entrapped into this structure, causing a high buoyancy and then bringing the flocs to the bitumen froth. Since we only observed a marginal difference in settling rate of tailings with the varied addition of the polymer, it appears that there is no clear difference in the flocculation of the tailings slurry at room temperature (Figure 6.3).

6.2 Results from procedure II

In procedure II, the polymer was first added to oil sands slurry (i.e. oil sands ore in Aurora plant process water) at room temperature. The conditioning of the oil sands slurry was then conducted at this temperature. After the conditioning, the oil sands slurry was heated to 40°C. Air bubbles were then introduced and bitumen flotation was conducted at 40°C. The procedure is similar to the settling procedure B. Figure 6.4 shows the bitumen recovery as a function of the polymer dosage at 40°C. When the polymer dosage increased from 0 to 400 ppm, the bitumen recovery after one hour flotation increased from 40% to 66%. Figure 6.5 shows the froth quality measured by B/S and B/W. The froth quality was deteriorated by the added polymers, indicating that the contents of solids and water in bitumen froth were increased with the polymer addition. The increased bitumen recovery could be attributed to the conformation change of the polymer when temperature increased from room temperature to 40°C. At room temperature (i.e. the conditioning temperature), the polymer has a long, extended conformation. The polymer can absorb on the surface of the fines by hydrogen bonding (Peng and Di, 1994; Long et al., 2006). When temperature increased to 40°C (i.e. the flotation temperature), the polymer became coiled. The fines were brought together by the polymer, forming dense flocs. For those large dense flocs, they will settle to the tailings slurry. However, the small flocs formed by the polymer with low molecular weights were possible to adsorb to the surface of bitumen or air bubbles, causing the froth quality decreased at 40°C. As the fines were effectively flocculated by the polymer at 40°C, the fine content was drastically reduced in the flotation process. The

overall attachment efficiency between the bitumen droplet and air bubbles was therefore improved, resulting in a higher bitumen recovery.

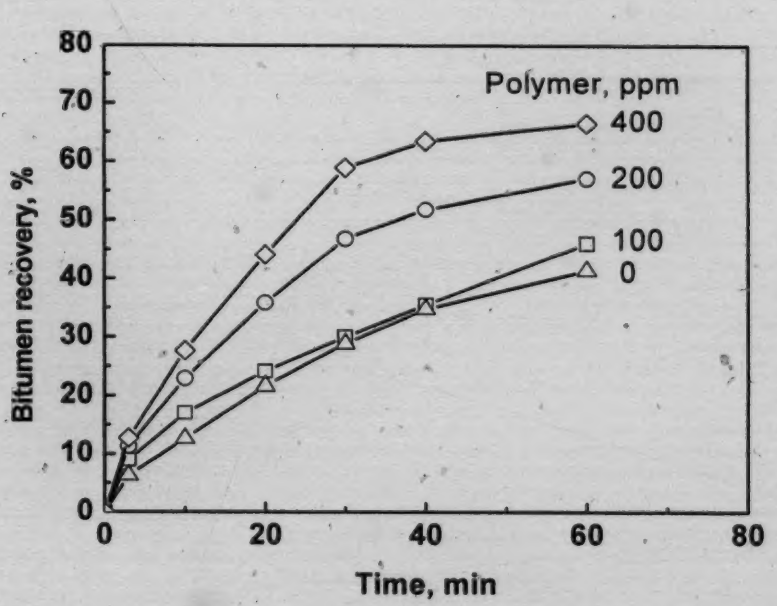

Figure 6.4 Bitumen recovery at various polymer dosages using extraction procedure II (i.e. bitumen flotation was conducted at 40°C).

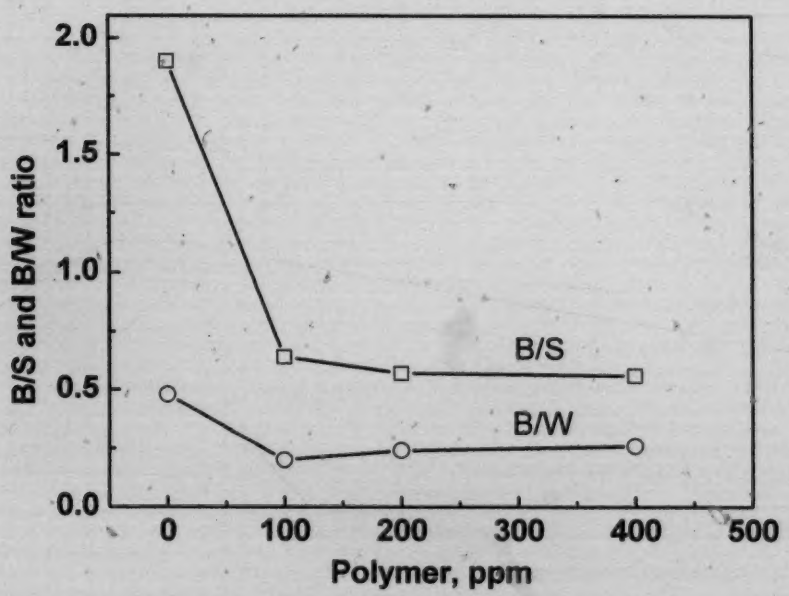

Figure 6.5 Bitumen froth quality (B/S and B/W) at various polymer dosages at 40°C.

After bitumen extraction, an oil sands tailings sample was directly taken to conduct the settling tests in a water bath at 40°C. Figure 6.6 shows the settling curves. With the polymer addition, the sediment volume decreased drastically. Figure 6.7 shows the initial settling rate as a function of the polymer dosage. When the polymer dosage was increased from 0 to 400 ppm, the initial settling rate increased from 0.2 to 2.5 m/h. The photograph of Figure 6.8 shows the settling results of the tailings after a settling time of 10 minutes at 40°C. A clear supernatant was observed at the polymer dosage of 400 ppm. In contrast, no clear supernatant was observed in the absence of the polymer. The improvement in the flocculation of the tailings slurry with the polymer addition can be attributed to the formation of large dense flocs at 40°C. The significance

of the settling results is that they reveal the effectiveness of the temperature-sensitive polymer on tailings treatment when the polymer was initially added in bitumen extraction stage. The water in the tailings could be released and then recycled immediately after flotation.

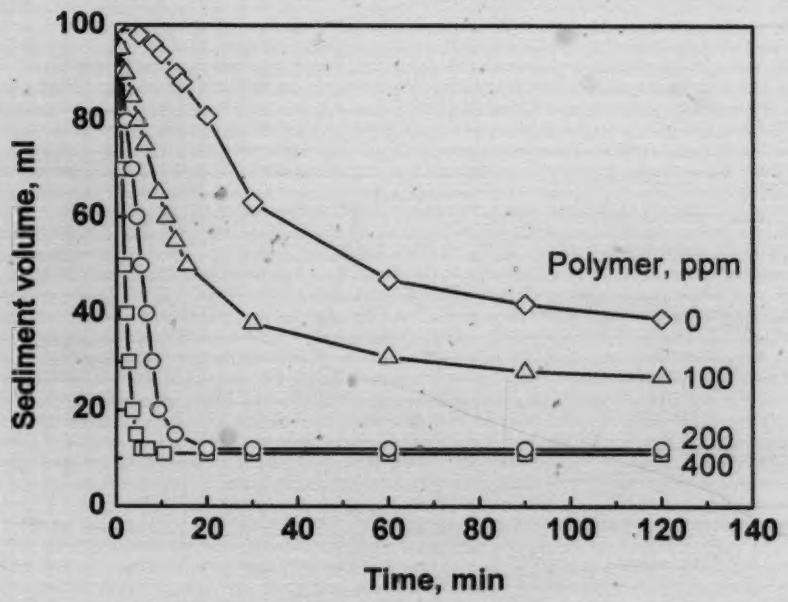

Figure 6.6 Settling curves of oil sands tailings at various polymer dosages and settling temperature of 40°C.

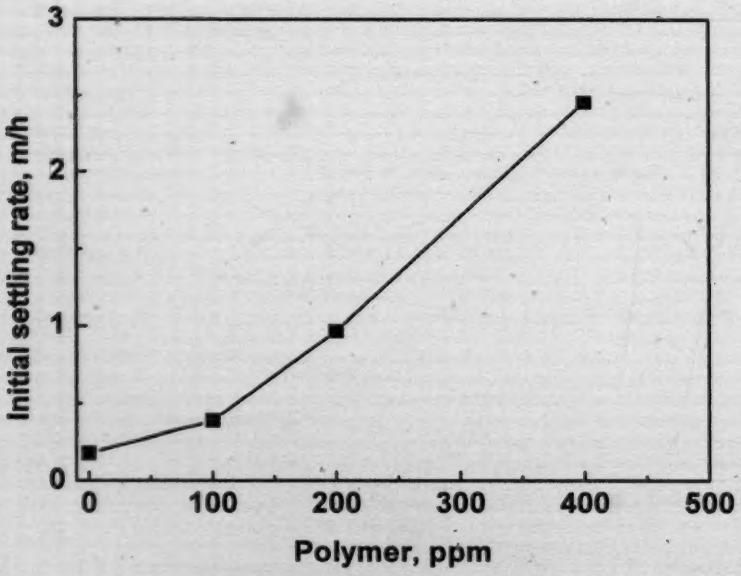

Figure 6.7 Initial settling rates of oil sands tailings as a function of polymer dosage at 40°C.

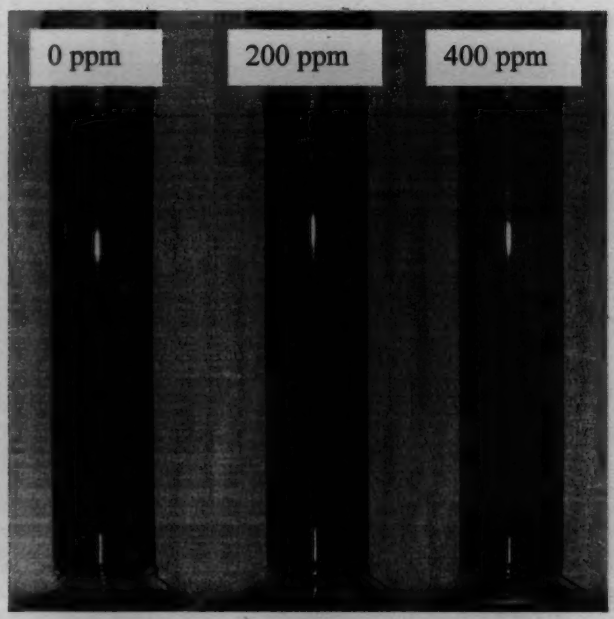

Figure 6.8 A photo showing tailings settling with various polymer addition at 40°C.

6.3 Summary

1. Extraction temperature has an important impact on bitumen recovery, froth quality, and tailings settling when a temperature-sensitive polymer was used as a process aid.

2. Using extraction procedure I, the addition of the polymer resulted in a reduction in bitumen recovery. Using extraction procedure II, the addition of the polymer resulted in a higher bitumen recovery as well as fast tailings settling.

Chapter 7 Conclusions

In this study, a temperature-sensitive polymer (poly(NIPAM)) was synthesized and used as a flocculant to treat clay suspensions and as a process aid for a low-grade oil sands ore processing. Two different procedures (procedures A/B or I/II) were employed in the settling experiments and extraction experiments. In the settling tests, for procedure A both mixing and settling were carried out at room temperature. For procedure B, mixing was carried out at room temperature and settling was conducted at a higher temperature of 40°C. In the extraction tests, for procedure I both conditioning of oil sands slurry and bitumen flotation were carried out at room temperature. For procedure II, the oil sands slurry conditioning was first carried out at room temperature and bitumen flotation was then conducted at 40°C. From this study, the following conclusions can be drawn.

(1) Temperature plays an important role in the settling of clay suspensions and bitumen extraction when the temperature-sensitive polymer (poly(NIPAM)) was used. In the settling of kaolinite suspensions, a better flocculation was obtained using procedure B than procedure A. In the bitumen extraction, a higher bitumen recovery and fast tailings settling were obtained using procedure II.

(2) The improvement in the flocculation of kaolinite suspensions or in the processing of low-grade oil sands ore was attributed to the molecular conformation change of the polymer with changing temperature. At room temperature the polymer has a long, extended structure while it becomes coiled at 40°C.

(3) Results for AFM force measurements were consistent with the settling test results. A weaker long-range repulsive force and a stronger adhesion force between kaolinite particles were obtained at 40°C.

(4) There exists a clear correlation between the measured adhesion forces between two clay particles and flocculation performance of the temperature-sensitive polymer: the higher, the adhesion force; the higher, the initial settling rate.

Chapter 8 Recommendations for future study

(1) Surface forces between two fines, fine and bitumen should be measured in the practical supernatants after bitumen extraction at both room temperature and 40°C.

(2) The measured colloidal forces should be correlated to the extraction test results.

(3) The adaptability of the polymer to different oil sands ores (e.g. good processing ore) should be investigated.

(4) Role of process water effect should be further studied.

(5) Molecular weight effect of the polymer should be studied.

References

Abraham, T.; Christendat, D.; Xu, Z.; Masliyah, J.; Gohy, J. F.; and Jérôme, R., "Role of polyelectrolyte charge density in tuning colloidal forces", *AIChE Journal*, 50(10), 2613-2626, 2004.

Ali, L. H., "Method for the Determination of Elemental Sulfur in Bitumen", *Fuel*, 54(4), 241-244, 1975.

Atago, Y.; Maruyama, T.; Kido, O.; and Oka, H., "Temperature-sensitive Flocculating Agents", *Jpn. Kokai Tokkyo Koho*, 4, 1992.

Attia, Y. A.; Deason, D.M., "Control of Slimes Coating in Mineral Suspensions", *Colloids Surf.*, 39, 227-238, 1989.

Baptista, M. V.; and Bowman, C. W. 19th Can. Chem. Eng. Conf., Edmonton, Alberta, 1969.

Basu, S.; Nandakumar, K.; Lawrence, S.; Masliyah, J., "Effect of Calcium Ion and Montmorillonite Clay on Bitumen Displacement by Water on a Glass Surface", Fuel, 83(1), 17-22, 2003.

Caughill, D. H., Scott, J. D., Liu, Y., Burns, R., and Shaw, W. H., Proceedings of the 47th Canadian Geotechnical Conference, Halifax, September 1993.

Chalaturnyk, R.J.; Scott,J.D.; Özüm, Baki., "Management of Oil Sands Tailings", *Petroleum Science and Technology*, 20(9 & 10), 1025-1046, 2002.

Chiaki, I., and Shiyuuji, S., "Solid/Liquid Separation Method of Suspension", *Japanese patent: 2001-232104*, 2001.

Claesson, P.M.; Blom, C.E.; Herder P.C.; and B.W. Ninham, "Interactions between Water-stable Hydrophobic Langmuir-Blodgett Monolayers on Mica", *J. Colloid Interface Sci.* 114, 234-242, 1986.

Clark, K.A.; and Pasternack, D.S., "Hot-water Separation of Bitumen from Alberta Bituminous Sand", *Journal of Industrial and Engineering Chemistry*, 24, 1410-1416, 1932.

Cuddy, G., "Empirical Studies on the Relationship between Process Water Chemistry and Oilsands Processability", *CONRAD Extraction Fundamentals*, March 28, 2000.

Cymerman, G.; Kwong, T.; Lord, E.; Hamza, H.; Xu, Y. "Polymers in Mineral Processing, Proceedings of the UBC-McGill Bi-Annual International Symposium on Fundamentals of Mineral Processing", Quebec City, QC, Canada, Aug. 22-26, 605-619, 1999.

Dai, Q.; Chung, K. H.; and Czamecki, J., "Formation of Calcium Carbonate in the Bitumen/Aqueous Sodium Hydroxide System", *AOSTRA J.*, 8(2), 95-101, 1992.

de Gennes, P.G., "Polymers at an Interface – A Simplified View", *Adv Colloid Interface* 27, 189-209, 1987.

Deng, Y.; Xiao, H.; and Pelton, R., "Temperature-Sensitive Flocculants Based on Poly(N-isopropylacrylamide-co-diallyldimethylammonium Chloride)", *Journal of Colloid and Interface Science*, 179, 188-193, 1996.

Derjaguin, B.V. *Kolloid Zeits.* 69, 155-164, 1934.

Derjaguin, B.V., Muller, V. M., and Toporov, Y. P. *J. Colloid Interface Sci.* 53, 314-326, 1975.

Ducker, W. A.; Senden, T. J.; and Pashley, R. M., "Measurement of Forces in Liquids Using a Force Microscope", *Langmuir*, 8, 1831-1836, 1992.

Dzinomwa, G. P. T.; Wood, C. J.; and Hill, D. J. T., "Fine Coal Dewatering Using pH- and Temperature-sensitive Superabsorbent Polymers", *Polymers for Advanced Technologies*, 8, 767-772, 1997.

Fujishige, S., "Intrinsic Viscosity-Molecular Weight Relationships for Poly (N - isopropylacrylamide) Solutions", *Polym. J.*, 19, 297-300, 1987.

Grahame, D.C. "The Electrical Double Layer and the Theory of Electro-capillarity", *Chemical Review*, 41, 441-501, 1947.

Graig, V.S.J.; Ninham B.W.; and R.M. Pashley, "Direct Measurement of Hydrophobic Forces: A Study of Dissolved Gas, Approach Rate, and Neutron Irradiation", *Langmuir* 15, 1562-1569, 1999.

Guillet, J.E.; Heskins, M.; and Murray, D.G., "Polymeric Flocculants", *U.S. Patent 4536294*, 1985.

Igarashi, C.; and Sakohara, S., "Solid-Liquid Separation Method for Suspension Using Heat Sensitive Polymer Flocculant", *Jpn. Kokai Tokkyo Koho*, 8, 2000.

Igarashi, C.; and Sakohara, S., "Separation of Solid and Liquid in Suspensions Using Ionic Temperature-Sensitive Polymer Flocculants", *Japanese Patent 2001-232104*, 2001.

Israelachvili, J.N. *Intermolecular and Surface Forces*, 2nd Ed. Academic Press, San Diego, 1992.

Israelachvili, J.N., and Pashley, R.M. "Measurement of the Hydrophobic Interaction between 2 Hydrophobic Surfaces in Aqueous-electrolyte Solutions", *J Colloid Interface Sci.* 98, 500-514, 1984.

Hepler, L.G.; and His, C., "AOSTRA Technical Handbook on Oil Sands, Bitumen and Heavy Oils", *AOSTRA technical publication series 6*, Alberta Oil Sands Technology and Research Authority, Edmonton, Canada, 1989.

Hepler, L.G., and Smith, R.G., "The Alberta Oil Sands: Industrial Procedures for Extraction and Some Recent Fundamental Research", *AOSTRA technical publication series 14*, Alberta Oil Sands Technology and Research Authority, Edmonton, AB, 1994.

Heskins, M., and Guillet, J.E., "Solution Properties of Poly(N-isopropylacrylamide)", *J. Macromol. Sci. Chem. A2*, 1441-1451, 1968.

Hogg, R.I., Healy, T.W., and Fuerstenau, D.W., "Mutual coagulation of colloidal dispersions", *Trans. Faraday Soc.*, 62, 1638-1651, 1966.

Hunter, J. R., *Introduction to Modern Colloid Science*, Oxford Univ. Press, New York, 1993.

Johnson, K.L.; Kendall, K. and Roberts, A.D. *Proc. R. Soc. London, Ser. A* 324, 301-313, 1971.

Kanazawa, H., "Temperature-Responsive Polymers for Liquid-Phase Separations", *Anal Bioanal Chem.*, 378, 46-48, 2004.

Kasongo, T.; Zhou, Z.A.; Xu, Z.; and Masliyah, J., "Effect of Calcium Ions and Fine Clays on Bitumen Extraction from Athabasca Oil Sands Using Flotation", *Can. J. Chem. Eng.*, 78, 674-681, 2000.

Katsumoto, Y.; Tanaka, T.; and Ozaki, Y., "Relationship between the Coil-Globule Transition of an Aqueous Poly(N-isopropylacrylamide) Solution and Structural Changes in Local Conformations of the Polymer", *Macromol. Symp.*, 205, 209-223, 2004.

Klimpel, R. R., "Introduction to Chemicals Used in Particle System", *ERC Particle Science & Technology,* In structural Module Series, Series Editor, Raj Rajagopalan, University of Florida, Gainesville, FL, 1997.

Li, H.; Long, J.; Xu, Z.; and Masliyah, J.H., "Synergetic Role of Polymer Flocculant in Low-Temperature Bitumen Extraction and Tailings Treatment", *Energy & Fuels*, 19(3), 936-943, 2005a.

Li, H.; Zhou, Z. A.; Xu, Z.; and Masliyah, J., "Role of Acidified Sodium Silicate in Low Temperature Bitumen Extraction from Poor-Processing Oil Sand Ores", *Industrial & Engineering Chemistry Research*, 44(13), 4753-4761, 2005b.

Li, H.; Long, J.; Xu, Z., and Masliyah, J. "Flocculation of Kaolinite Suspension Using a Temperature-Sensitive Polymer", Submitted to AIChE J., 2006.

Liu, J. F.; Min, G.; and Ducker, W. A., "AFM Study of Adsorption of Cationic Surfactants and Cationic Polyelectrolytes at the Silica-Water Interface", *Langmuir*, 17, 4895-4903, 2001.

Liu, J. "Role of Colloidal Interactions in Bitumen Recovery from Oil sands", Ph.D Dissertation, University of Alberta, 2004.

Liu, J.; Xu, Z.; and Masliyah, J. H., "Studies on Bitumen-Silica Interaction in Aqueous Solutions by Atomic Force Microscopy", *Langmuir*, 19, 3911-3920, 2003.

Liu, J.; Xu, Z.; and Masliyah, J. H., "Role of Fine Clays in Bitumen Extraction from Oil Sands", *AIChE J.*, 50, 1917-1927, 2004a.

Liu, J., Xu, Z., and Masliyah, J., "Interaction between Bitumen and Fines in Oil Sands Extraction System: Implication to Bitumen Recovery", *Canadian Journal of Chemical Engineerin*, 82(4), 655-666, 2004b.

Liu, J.; Xu, Z.; and Masliyah, J., "Interaction Forces in Bitumen Extraction from Oil Sands", *Journal of Colloid and Interface Science*, 287, 507-520, 2005a.

Liu, J.; Xu, Z.; and Masliyah, J., "Colloidal Forces between Bitumen Surfaces in Aqueous Solutions Measured with Atomic Force Microscope", *Colloids and Surface A: Physicochem. Eng. Aspects*, 260, 217-228, 2005b.

Liu, J., Zhou, Z., Xu, Z., and Masliyah, J. "Bitumen-Clay Interactions in Aqueous Media Studied by Zeta Potential Measurement", J. Colloid Interface Sci. 252:409-418, 2002.

Long, J.; Li, H.; Xu, Z.; and Masliyah, J.H., "Role of Colloidal Interactions in Oil Sand Tailings Treatment", *AIChE J.*, 52, 371-383, 2006.

Mackinnon, M. D.; Matthews, J. G.; Show, W. H.; and Cuddy, R. G., "Water Quality Issues Associated with Composite Tailings (CT) Technology for Managing Oil Sands Tailings", *International Journal of Surface Mining, Reclamation and Environment*, 15(4), 235-256, 2001.

Masliyah, J.; Long, J.; and Xu, Z., "Colloidal Interactions and Stability of Clay Suspensions", 229th ACS National Meeting, San Diego, CA, United States, 2005.

Masliyah, J.H. *Electrokinetic Transport Phenomena*, AOSTRA Series #12, University of Alberta, Edmonton, Canada, 1994.

Matthews, J. G.; Shaw, W. H.; MacKinnon, M. D.; and Cuddy, R. G., "Development of Composite Tailings Technology at Syncrude", *International Journal of Surface Mining, Reclamation and Environment*, 16(1), 24-39, 2002.

Mikula, R.; Munoz, V.A.; Lam, W.W.; Payette, C.; and MacConnachie, C.A. "Structure and Drying Behavior of Oil Sands Fine Tails: The Effect of Clay Type and Water Chemistry", *Proc. Oil Sands- Our Petroleum Future*, Edmonton, April 4-7, 1993.

Misra, M.; Aguilar, R.; and Miller, J. D., "Surface Chemistry Features in the Hot Water Processing of Utah Tar Sand", *Separation Science and Technology*, 16(10), 1523-1544, 1981.

Mpofu, P.; Addai-Mensah, J.; and Ralston, J., "Investigation of the Effect of Polymer Structure Type on Flocculation, Rheology and Dewatering Behaviour of Kaolinite Dispersions", *Int. J. Miner. Process.*, 71, 247-268, 2003.

Mpofu, P.; Addai-Mensah, J.; and Ralston, J., "Temperature Influence of Nonionic Polyethylene Oxide and Anionic Polyacrylamide on Flocculation and Dewatering Behavior of Kaolinite Dispersions", *J. Colloid and Interface Sci.*, 271(1), 145-156, 2004(a).

Mpofu, P.; Addai-Mensah, J.; and Ralston, J., "Flocculation and Dewatering Behaviour of Smectite Dispersions: Effect of Polymer Structure Type", *Minerals Engineering*, 17, 411-423, 2004(b).

Peng, F. F.; and Di, P., "Effect of Multivalent Salts-Calcium and Aluminum on the Flocculation of kaolin Suspension with Anionic Polyacrylamide", *J. Colloid Interface Sci.*, 164, 229-237, 1994.

Pradip; Ravishankar, S. A.; Sankar, T. A. P.; and Khosla, N. K., " Benefaction Studies on Alumina-Rich Indian iron Ore Slimes Using Selective Didpersants, Flocculants and Flotation Collectors", Proceedings:XVIII International Mineral Processing Congress, Sydney, Australia, 1993.

Pincus, P. "Colloid Stabilization with Grafted Polyelectrolytes", *Macromolecules* 24, 2912-2919, 1991.

Rabinovich, Y. I.; and Yoon, R. H., "Use of Atomic Force Microscope for the Measurements of Hydrophobic Forces between Silanated Silica Plate and Glass Sphere", *Langmuir*, 10, 1903-1909, 1994.

Ramachandram, R.; Somasundaran, P. "Effect of temperature on the interfacial properties of silicates", *Colloids and Surfaces* 21, 355-369, 1986.

Ramon, O.; Kesselman, E.; Berkovici, R.; Cohen, Y.; and Paz, Y. J., "Attenuated Total Reflectance/Fourier Transform Infrared Studies on the Phase-Separation Process of Aqueous Solutions of Poly(N-isopropylacrylamide)", *Polym. Sci. Part B: Polym. Phys.*, 39, 1665-1677, 2001.

Richard J. Chalaturnyk; J. Don Scott; and Baki Özüm, "Management of Oil Sands Tailings", *Petroleum Science and Technology*, 20(9&10), 1025-1046, 2002.

Sakohara, S.; Kimura, T.; and Nishikawa, K., "Flocculation Mechanism of Suspended Particles Utilizing Hydrophilic/Hydrophobic Transition of Thermo-Sensitive Polymer", *Kagaku Kogaku Ronbunshu*, 26(5), 734-737, 2000.

Sakohara, S.; and Nishikawa, K., "Flocculation and Compaction of Highly Concentrated Suspension Using Thermo-Sensitive Polymers", *Kagaku Kogaku Ronbunshu*, 26(2), 298-304, 2000.

Sakohara, S.; and Nishikawa, K., "Compaction of TiO_2 Suspension Utilizing Hydrophilic/Hydrophobic Transition of Cationic Thermo-Sensitive Polymers", *J. Colloid and Interf. Sci.*, 278, 304-309, 2004.

Sanford, E. C.; and Seyer, F. A., "Batch Extraction Unit for Tar Sand Processing Studies", *Preprints of Papers - American Chemical Society, Division of Fuel Chemistry*, 23(4), 54-62, 1978.

Sanford, E.C.; and Seyer, F.A., "Processibility of Athabasca Tar Sand Using a Batch Extraction Unit: The Role of NaOH", *CIM Bulletin* 72(803), 164-169, 1979.

Sanford, E. C., "Processability of Athabasca Oil Sand: Interrelationship between Oil Sand Fine Solids, Process aids, Mechanical Energy and Oil Sand Age after Mining", *Canadian Journal of Chemical Engineering*, 61(4), 554-67, 1983.

Schild, H.G., "Poly(N-isopropylacrylamide): Experiment, Theory and Application", *Prog. Polym. Sci.*, 17, 163-249, 1992.

Schramm, L. L.; Smith, R. G.; and Stone, J. A., "The Infuence of Natural Surfactant Concentration on the Hot Water Process for Recovering Bitumen fron the Athabasca Oil Sands", *AOSTRA J. Res.* 1(1), 5-13, 1984.

Schramm, L. L.; Stasiuk, E. N.; and MacKinnon, M., *Surfactants*, pp: 365-430. Publisher: Cambridge University Press, Cambridge, UK, 2000.

Scott, J. D.; Bill, Y.; and Caughill, D. L., Proceedings of Oil Sands- Our Petroleum Future Conference, Edmonton, Alberta, Canada, Apr.4-7, 1993.

Sethi, A., "Applicability of the OHWE process to Suncor OSG", Suncor report by MMRT, Fort McMurray, 1993.

Škvarla, J. " Hydrophobic Interaction between Macroscopic and Microscopic Surfaces. Unification Using Surface Thermodynamics", *Advances in colloid and interface science* 91, 335-390, 2001.

Smith, R. G.; and Schramm, L. L., "The Influence of Mineral Components on the Generation of Natural Surfactants from Athabasca Oil Sands in the Alkaline Hot Water Process", *Fuel Process. Technol.*, 30, 1-14, 1992.

Smith, R.G., and Ng, S., "Towards a Model for the Prediction of Fine Tails Volume", Oil Sands – Our Petroleum Future Conference, Edmonton, Alberta, April 4-7, 1993.

Speight, J. G.; and Moschopedis, S. E., "Factors Affecting Bitumen Recovery by the Hot Water Process", *Fuel Processing Technology*, 1(4), 261-8, 1978.

Stern, Otto. "The Theory of the Electrolytic Double-Layer", *Zeitschrift Fuer Elektrochemie und Angewandfe Physikalische Chemie*, 30, 508-516, 1924.

Stuart, B.H. *Polymer Analysis*. Chichester; New York: J. Wiley, 2002.

Sworska, A.; Laskowski, J. S.; and Cymerman, G., "Flocculation of the Syncrude Fine Tailings. Part I. Effect of pH, Polymer Dosage and Mg^{2+} and Ca^{2+} Cations", *Int. J. Miner. Process.*, 60, 143-152, 2000.

Syncrude Analytical Methods of Oil Sands and Bitumen, Syncrude Canada Ltd., Edmonton, AB, 1979.

Takamura, K.; and Wallace, D., "Experimental and Theoretical Studies of the Hot Water Processability of Different Grades of Athabasca Oil Sands", *Process Technology Proceedings*, 4, 579-98, 1987.

Takamura, K.; and Wallace, D., "The Physical Chemistry of the Hot Water Process", *Can. J. Petro. Tech.*, 27, 98-106, 1988.

Tipman, R., "Muskeg River Pilot Plant Experience with Poorly Processing Ores", *CONRAD Extraction Fundamentals*, March 28, 2000.

Wallwork, V.; Xu. Z.; and Masliyah, J., "Bitumen Recovery with Oily Air Bubbles", *Canadian J. Chem. Eng.*, 81, 993-997, 2003.

Warszynski, P.; and Adamczyk, Z., "Calculations of Double-Layer Electrostatic Interactions for the Sphere/Plane Geometry", *J. Colloid Interface Sci.*, 187, 283, 1997.

White, L.R., "On the Derjaguin approximation for the interaction of macrobodies", *J. Colloid Interface Sci.*, 95,286-288, 1983.

Wu, X. Y.; Zgabg, Q.; and Arshady, R., "Stimuli Sensitive Hydrogels: Polymer Structure and Phase Transition", *PBM Series*, Volume 1, 157-194, 2003.

Xu, Y.; and Hamza, H., "Thickening and Disposal of Oil Sand Tailings", *Mining Engineering*, 55(11), 33-39, 2003.

Xu, Y.; Hamza, H.; and Matthews, J., Particle Size Enlargement in Mineral Processing, Proceedings of the 5th UBC-McGill Biennial International Symposium on Fundamentals of Mineral Processing, Hamilton, ON, Canada, Aug. 22-25, 271-288, 2004.

Zareie, H. M.; Volga Bulmus, E.; Gunning, A.P.; Hoffman, A.S.; Piskin, E.; and Morris, V.J., "Investigation of a Stimuli-Responsive Copolymer by Atomic Force Microscopy", *Polyme*, 41, 6723-6727, 2000.

Zhao, H.; Long, J.; Xu, Z.; and Masliyah, J. "Effects of Divalent and Surfactants on Silica-Bitumen Extraction" *Industrial Engineering Chemistry Research*, 45(22), 7482-7490, 2006.

Zhou, Z. A.; Xu, Z.; Masliyah, J.; Czarnecki, J., "Coagulation of Bitumen with Fine Silica in Model Systems", *Colloids and Surface A: Physicochemical and Engineering Aspects*, 148(3), 199-211, 1999.

Appendix: Numerical solution to DLVO theory (Liu, 2004)

A: Constant Stern potential as B.C. - general purpose routine

Step 1: Numerical solution to non-linear Possion-Boltzman equation

Possion-Boltzman equation can be re-arranged as:

$$\frac{d^2\psi}{dx^2} = f(\psi), \text{ With } f(\psi) = -\frac{e}{\varepsilon\varepsilon_0}\sum_j z_j n_{j\infty} e^{-z_j e\psi / kT}$$

$$\text{B.C. } \begin{cases} \psi_0 \equiv \psi_a \\ \psi_n \equiv \psi_b \end{cases}$$

Where j is the type of ion j in the solution.

Assuming that the separation between two plates a and b was evenly divided into n steps with step size h, the differential equation can be expanded numerically.

$$h = \frac{x_n - x_0}{n}$$

Using central difference with even spaced to expand left side:

$$\frac{d^2\psi(x_i)}{dx^2} = \frac{\psi_{i+1} - 2\psi_i + \psi_{i-1}}{h^2}, \text{ i=0,1, 2...n}$$

Using Newton method to expand right side:

$$f(x_i,\psi_i) = f(x_i,\psi_i^m) + f_\psi'(x_i,\psi_i^m)(\psi_i - \psi_i^m), \text{ i=0,1, 2...n}$$

then we can get a set of linear equations:

$$\begin{bmatrix} d_1 & 1 & & & & & \\ 1 & d_2 & 1 & & & & \\ & \ddots & \ddots & \ddots & & & \\ & & 1 & d_i & 1 & & \\ & & & \ddots & \ddots & \ddots & \\ & & & & 1 & d_{n-2} & 1 \\ & & & & & 1 & d_{n-1} \end{bmatrix} \begin{bmatrix} \psi_1 \\ \psi_2 \\ \vdots \\ \psi_i \\ \vdots \\ \psi_{n-2} \\ \psi_{n-1} \end{bmatrix} = \begin{bmatrix} b_1 \\ b_2 \\ \vdots \\ b_i \\ \vdots \\ b_{n-2} \\ b_{n-1} \end{bmatrix}$$

With boundary: $\begin{cases} \psi_0 = \psi_a \\ \psi_n = \psi_b \end{cases}$

in which :

$$d_i = -2 - h^2 f'_{\psi}(x_i, \psi_i^m), \quad \text{i=1,2,---, n-1}$$

$$b_i = h^2 f(x_i, \psi_i^m) - h^2 f'_{\psi}(x_i, \psi_i^m)\psi_i^m, \qquad \text{i=2, 3 --, n-2}$$

$$b_1 = -\psi_0 + h^2 f(x_1, \psi_1^m) - h^2 f'_{\psi}(x_1, \psi_1^m)\psi_1^m$$

$$b_{n-1} = -\psi_n + h^2 f(x_{n-1}, \psi_{n-1}^m) - h^2 f'_{\psi}(x_{n-1}, \psi_{n-1}^m)\psi_{n-1}^m$$

with initial guess $\underline{\psi^m}$, use Thomas Algorithm to solve this matrix equation until the convergence is OK.

Using this procedure, the surface potential distribution $\psi(x)$ between two plates can be obtained.

Step2: Numerical solution to osmotic pressure

First, the central difference to calculate the surface potential:

$$\frac{d\psi(x_i)}{dx} = \frac{\psi(x_{i+1}) - \psi(x_{i-1})}{2h} \quad \text{i=2, 3, ...n-1.}$$

Then the pressure at separation of D can be calculated at middle plane:

$$P(D) = kT\sum_i (n_i - n_{i\infty}) - \frac{\varepsilon\varepsilon_0}{2}\left(\frac{d\psi(x_{n/2})}{dx}\right)^2 = kT\sum_i n_{i\infty}(e^{-z_i e\psi(x_{n/2})/kT} - 1) - \frac{\varepsilon\varepsilon_0}{2}\left(\frac{d\psi(x_{n/2})}{dx}\right)^2$$

Step 3: Numerical solution to electric double layer energy

The interaction energy between two plates can be calculated by use of Trapezoidal rule:

$$U_E = -\int_{\infty}^{D} P(x)dx = \int_{D}^{\infty} P(h)dh = \frac{1}{2h}\sum_{j=i}^{\infty}(P_j + P_{j+1}) = \frac{1}{2h}(P_i + 2\sum_{j=i+1}^{\infty} P_j + P_n) \quad \text{per unit}$$

Step 4: Numerical solution to van der Waals energy

Step 5: Convert interaction energy to interaction force using equation as $F = 2\pi\sqrt{R_A R_B}U_{p-p}$. For the system of sphere (R_1)-sphere (R_2): $R_A = R_B = \frac{R_1 R_2}{R_1 + R_2}$,

$$F_{s-s} = 2\pi\frac{R_1 R_2}{R_1 + R_2}U_{p-p}.$$

The full Visual Basic code for DLVO theory was given in the following. The information about boundary condition, electrolyte (concentration and valence) and Hamaker constant has to be given. The other parameters including the temperature and points of step are optional. If these optional parameters are not chosen, the code will

automatically choose room temperature 22^0C and 101 points for the calculation. The points of step are only related to the accuracy of this method itself, and have nothing to with data fitting. Usually 100 to 400 points are used, with the larger the points of step resulting in a more accuracy of the results. Other parameters such as electrolyte concentration and surface potential are used for data fitting. First, the electrolyte concentrations are changed to fit the decay length of interaction force at larger separation (20 ~100 nm). Then the surface potentials are altered to fit the magnitude of interaction force.

```
Option Base 1
Option Explicit
'This code is designed to calculate the DLVO theory by Jianjun Liu, Zhenghe Xu

Function DLVO(Potentialbound, C, Z, Ha, Optional n As Integer = 11, Optional
xbound As Double = 110, Optional T As Double = 25, Optional tol As Double =
0.000000001)
Dim Ve() As Double, Vtotal() As Double, h As Double, i As Integer, j As Integer, tem()
As Double
ReDim Ve(n, 4), Vtotal(n, 11), tem(n)   ' Ve
h = xbound / 1000000000# / (n - 1)   ' stepsize

'Claculate the separation  Vtotal(i,1), nm
For i = 1 To n
 Vtotal(i, 1) = (i - 1) * h * 1000000000#
Next i

' calculate the electric force Vtotal(i, 2) for plate-plate
For i = 2 To n
 Call Velect(Ve, Vtotal(i, 1), Potentialbound, C, Z, n, T, tol)
 Vtotal(i, 2) = Ve(n / 2, 4)
Next i

'calculate the electric energy Vtotal(i, 3) for plate-plate
For i = 1 To n
 tem(i) = 0#
For j = i + 1 To n - 1
 tem(i) = tem(i) + Vtotal(j, 2)
Next j
 Vtotal(i, 3) = (h / 2# * (Vtotal(i, 2) + 2# * tem(i) + Vtotal(n, 2))) * 1000#
```

```
Next i

'calculate Vander Waals energy Vtotal(i, 4)
Dim Ham As Double
Ham = (Ha(1) ^ 0.5 - Ha(3) ^ 0.5) * (Ha(2) ^ 0.5 - Ha(3) ^ 0.5)
Vtotal(1, 4) = (-Ham / 12# / 3.14159 / 0.000000000001 ^ 2) * 1000#
For i = 2 To n
 Vtotal(i, 4) = (-Ham / 12# / 3.14159 / (Vtotal(i, 1) / 1000000000#) ^ 2) * 1000#  'for
plate-palte
Next i

'calculate the total force
For i = 1 To n
Vtotal(i, 5) = 2# * 3.14159 * (Vtotal(i, 3) + Vtotal(i, 4))
Next i

Dim tep() As Double
ReDim tep(n, 4)
For i = 1 To n
tep(i, 1) = Vtotal(i, 1)
tep(i, 2) = Vtotal(i, 5)
tep(i, 3) = Vtotal(i, 3) * 2# * 3.14159
tep(i, 4) = Vtotal(i, 4) * 2# * 3.14159
Next i
DLVO = tep
End Function
' claculate the surface potential distribution, surface potential differential & interaction
force between two plates
Sub Velect(Ve, xbound As Double, Potentialbound, C, Z, n As Integer, T As Double,
tol As Double)
Dim Ve0() As Double, A() As Double, b() As Double, h As Double
Dim i As Integer, sum1 As Double, sum2 As Double

ReDim Ve0(n - 2), A(n - 2, n - 2), b(n - 2), d(n - 2)
h = xbound / 1000000000# / (n - 1)

' calculate the zeta potential Ve(i,2), mv
Ve(1, 2) = Potentialbound(1)
Ve(n, 2) = Potentialbound(2)
For i = 1 To n - 2 ' initial guess
Ve0(i) = 0
Next i
Do
Call MatrixD(d, h, Ve0, n - 2, C, Z, T)   ' calculate the diangonle di
Call Martixb(b, h, Ve0, Potentialbound, n - 2, C, Z, T)  'calculate bi
Call Thomas(d, b, n - 2)    ' use Thomas method to solve the matrix equation
```

```
For i = 2 To n - 1
 Ve(i, 2) = b(i - 1) * 1000
Next i
sum1 = 0#
sum2 = 0#
For i = 1 To n - 2
 sum1 = sum1 + Abs(b(i) - Ve0(i))
 sum2 = sum2 + Abs(b(i))
Next i
If (sum1 / sum2 < tol) Then Exit Do    ' check the convergence
For i = 1 To n - 2
 Ve0(i) = b(i)
Next i
Loop

' claculate the potential diffenetial Ve(i,3), v/m
Ve(1, 3) = (Ve(2, 2) - Ve(1, 2)) / 1000# / h
Ve(n, 3) = (Ve(n, 2) - Ve(n - 1, 2)) / 1000# / h
For i = 2 To n - 1
Ve(i, 3) = (Ve(i + 1, 2) - Ve(i - 1, 2)) / 2000# / h
Next i

'calculate force Ve(i,4) @ middle plane
Dim m As Integer, F As Double, j As Integer
m = C.Count
For j = 1 To n
 F = 0
For i = 1 To m
 F = F + C(i) * (Exp(-Z(i) * 1.602E-19 * Ve(n / 2, 2) / 1000# / 1.38E-23 / (T + 273)) -
1#)
Next i
 Ve(j, 4) = 1.38E-23 * (T + 273) * 1000 * 6.03E+23 * F - 0.5 * 78.5 *
0.00000000000885 * Ve(n / 2, 3) ^ 2
Next j
End Sub

Sub MatrixD(d, h, y0, n As Integer, C, Z, T As Double)
Dim i As Integer
For i = 1 To n
  d(i) = -2# - h ^ 2 * Jac(y0(i), C, Z, T)
Next i

End Sub

Private Function Jac(Y, C, Z, T) As Double
Dim n As Integer, i As Integer, F As Double
```

```
n = C.Count
F = 0
For i = 1 To n
  F = F + C(i) * Z(i) ^ 2 * Exp(-Z(i) * 1.602E-19 * Y / 1.38E-23 / (T + 273))
Next i
Jac = F * (1000 * 6.03E+23) * (1.602E-19) ^ 2 / (1.38E-23 * (T + 273) * 78.5 *
0.00000000000885)
End Function

Sub Martixb(b, h, y0, Potenialbound, n, C, Z, T As Double)
Dim F() As Double, fy() As Double
ReDim F(n), fy(n)
Dim i As Integer
For i = 1 To n
 F(i) = Fun(y0(i), C, Z, T)
 fy(i) = Jac(y0(i), C, Z, T)
 b(i) = h ^ 2 * F(i) - h ^ 2 * fy(i) * y0(i)
Next i
 b(1) = -Potenialbound(1) / 1000# + b(1)
 b(n) = -Potenialbound(2) / 1000# + b(n)
End Sub

Private Function Fun(Y, C, Z, T) As Double
Dim n As Integer, i As Integer
n = C.Count
For i = 1 To n
Fun = Fun - (1000 * 6.02E+23) * 1.602E-19 / (78.5 * 0.00000000000885) * (C(i) * Z(i)
* Exp(-Z(i) * 1.602E-19 * Y / 1.38E-23 / (T + 273)))
Next i
End Function

Sub Thomas(d, r, ByVal n As Integer, Optional ByVal ist As Integer = 1)
'This subroutine solves a set of tridiagonal linear equations using Thomas Algorithm
'd contains the diangular term
'Forward substitution

Dim i As Integer
For i = ist + 1 To n
  d(i) = d(i) - 1# / d(i - 1)
  r(i) = r(i) - 1# * r(i - 1) / d(i - 1)
Next i

'Backward substitution
r(n) = r(n) / d(n)
For i = n - 1 To ist Step -1
 r(i) = (r(i) - 1# * r(i + 1)) / d(i)
```

Next i

'Solution obtained successfully!
End Sub

B: Constant surface charge density as B.C. - general purpose routine

Possion-Boltzman equation can be re-arranged as:

$$\frac{d^2\psi}{dx^2} = f(\psi), \text{ with } \quad f(\psi) = -\frac{e}{\varepsilon\varepsilon_0}\sum_j z_j n_{j\infty} e^{-z_j e\psi / kT}$$

$$\text{B.C.} \quad \begin{cases} \dfrac{d\psi(x_0)}{dx} \equiv a, & \psi(x_0) = \psi_a \\ \dfrac{d\psi(x_n)}{dx} \equiv b, & \psi(x_n) = \psi_b \end{cases}$$

Step 1: Calculation of surface charge density:

Transfer the non-linear Possion-Boltzman equation into form of equation

$$\frac{d^2\psi}{dx^2} = \frac{1}{2}d(\frac{d\psi}{dx})^2 = -\frac{e}{\varepsilon\varepsilon_0}\sum_j z_j n_{j\infty} e^{-z_j e\psi / kT}$$

for a single particle, we can get the values of a and b from given surface potential ψ_0 by equation

$$\frac{d\psi}{dx} = \pm\sqrt{\frac{2000NkT}{\varepsilon\varepsilon_0}\sum_j C_{j\infty}(e^{-\frac{z_j e\psi_0}{kT}} - 1)}$$

Step 2: calculate the zeta potential distribution:

By guessing the initial values: $\begin{cases}\psi_0 = \psi_a \\ \psi_n = \psi_b\end{cases}$, the routine described in Appendix A is used to calculate the potential distribution $\psi(x_i)$ and differential potential distribution $\frac{d\psi(x_i)}{dx}$. Then check the convergence of $\left(|a| - \left|\frac{d\psi(x_o)}{dx}\right| + |b| - \left|\frac{d\psi(x_n)}{dx}\right|\right)$. If it is not converged, use new guess $\begin{cases}\psi_0 = \psi_a + ah \\ \psi_n = \psi_b + bh\end{cases}$ until it was converged.

The other steps are the same as Appendix A.